JCTC Journal of Chemical Theory and Computation

Hydrogen Abstraction Acetylene Addition and Diels−Alder Mechanisms of PAH Formation: A Detailed Study Using First Principles Calculations

V. V. Kislov,[†,‡] N. I. Islamova,[§] A. M. Kolker,[§] S. H. Lin,[‡] and A. M. Mebel*[,†]

Department of Chemistry and Biochemistry, Florida International University, Miami, Florida 33199, Institute of Atomic and Molecular Sciences, Academia Sinica, P.O. Box 23-166, Taipei 10764, Taiwan, and Institute of Solution Chemistry of Russian Academy of Sciences, Akademicheskaya St. 1, Ivanovo 153045, Russia

Received March 1, 2005

Abstract: Extensive ab initio Gaussian-3-type calculations of potential energy surfaces (PES), which are expected to be accurate within 1−2 kcal/mol, combined with statistical theory calculations of reaction rate constants have been applied to study various possible pathways in the hydrogen abstraction acetylene addition (HACA) mechanism of naphthalene and acenaphthalene formation as well as Diels−Alder pathways to acenaphthalene, phenanthrene, and pyrene. The barrier heights; reaction energies; and molecular parameters of the reactants, products, intermediates, and transition states have been generated for all types of reactions involved in the HACA and Diels−Alder mechanisms, including H abstraction from various aromatic intermediates, acetylene addition to radical sites, ring closures leading to the formation of additional aromatic rings, elimination of hydrogen atoms, H disproportionation, C_2H_2 cycloaddition, and H_2 loss. The reactions participating in various HACA sequences (e.g., Frenklach's, alternative Frenklach's, and Bittner and Howard's routes) are demonstrated to have relatively low barriers and high rate constants under combustion conditions. A comparison of the significance of different HACA mechanisms in PAH growth can be made in the future using PES and molecular parameters obtained in the present work. The results show that the Diels−Alder mechanism cannot compete with the HACA pathways even at high combustion temperatures, because of high barriers and consequently low reaction rate constants. The calculated energetic parameters and rate constants have been compared with experimental and theoretical data available in the literature.

1. Introduction

The formation of polycyclic aromatic hydrocarbons (PAHs) has become one of the central areas in combustion research because of the great environmental effect attributed to these compounds. Numerous studies have shown PAHs to be major air pollutants exhibiting mutagenic and tumorogenic activities.[1−3] Having been formed as a result of the incomplete combustion of fossil fuels, PAHs are present in our environment in the form of atmospheric aerosols, soot, and volatile particles, usually together with other airborne toxic chemicals.[4,5] The processes of fullerene and soot formation were shown to involve PAH intermediates at the initial stages of synthesis.[6,7] PAHs and their cations are also found to play an important role in interstellar chemistry.[8,9] According to different estimates, PAH molecules could account for 2−30% of the carbon in the galaxy and may provide nucleation sites for the formation of carbonaceous dust.[8] PAHs are also believed to be responsible for many emission features in

* To whom correspondence should be addressed. E-mail: mebela@fiu.edu.

† Florida International University.

‡ Institute of Atomic and Molecular Sciences, Academia Sinica.

§ Institute of Solution Chemistry of Russian Academy of Sciences.

10.1021/ct0500491 CCC: $30.25
Published on Web 06/21/2005

astronomical infrared spectra.[9] To help researchers and engineers to develop cleaner combustion equipment, which would minimize soot and PAH production, it is imperative to know the mechanisms, rate constants, and product yields for the reactions relevant to PAH synthesis. Experimental and theoretical studies of such mechanisms represent an important source of kinetic and thermodynamic data required for the modeling of complex combustion systems.

Three possible mechanisms relevant to the formation of PAH have been proposed and critically discussed by the combustion community in the past two decades. The first one is known as the hydrogen abstraction acetylene addition (HACA) mechanism. It was introduced by Frenklach and Wang[10] and represents a repetitive sequence of two principal reaction steps, the abstraction of a hydrogen atom from the reacting hydrocarbon by another hydrogen atom followed by the addition (or several additions) of acetylene molecules to the radical site formed in the previous H-abstraction step. The first step activates a singlet hydrocarbon molecule, producing a radical intermediate, which can be involved in further growth by the reaction with acetylene. The production of a higher PAH containing an extra aromatic ring in its core can be accomplished by a ring closure reaction. Two alternative HACA pathways for the sequential additions of two acetylene molecules were proposed by Frenklach et al.[11−13] and by Bittner and Howard.[14] In Frenklach's route, the second acetylene molecule adds to the aromatic ring activated by either a conventional or an internal[15] hydrogen abstraction mechanism, whereas in Bittner−Howard's route, the second acetylene molecule adds to the first one. Several high-level ab initio studies of some important HACA steps were carried out in recent years. The hydrogen abstraction reactions from benzene ($C_6H_6 + H \rightarrow C_6H_5 + H_2$, $C_6H_6 + OH \rightarrow C_6H_5 + H_2O$, and $C_6H_5 + CH_3 \rightarrow C_6H_6 + CH_4$) were studied employing Gaussian-2 and Gaussian-3 (G2 and G3, respectively) model chemistry methods combined with either Rice−Ramsperger−Kassel−Marcus (RRKM) or transition state theory (TST) calculations of rate constants.[16−19] The mechanism of acetylene addition to the phenyl radical was investigated by Tokmakov and Lin,[20] utilizing the G2M scheme to compute the potential energy surface (PES) for the reaction and RRKM theory to calculate reaction rates. However, up to now, there were no systematic and accurate ab initio/statistical theory studies for the complete HACA networks. Bauschlicher and Ricca.[21] computed barrier heights and reaction energies for numerous reaction steps involved in the HACA naphthalene synthesis using a rather modest B3LYP/4-31G level of theory. On the basis of their calculated PES, they concluded that both Frenklach's and Bittner−Howard's routes exhibit low barriers but could not determine which HACA route is the most favorable. In our previous B3LYP/6-31G* study of the HACA phenanthrene synthesis,[22] we computed PESs for all reactions involved in this network and calculated respective rate constants using the canonical transition state theory. Our results also indicated that both HACA routes are probable at combustion temperatures.

An alternative mechanism of PAH formation that does not involve acetylene molecules has been proposed by Miller and Melius on the basis of a series of flame experiments combined with kinetic modeling.[23−25] They introduced several pathways leading to benzene and naphthalene starting from recombination products of two propargyl (C_3H_3)[23] or two cyclopentadienyl (C_5H_5)[24] radicals, respectively. Both propargyl and cyclopentadienyl radicals were shown to be highly abundant in hydrocarbon flames and to play an important role in combustion chemistry.[6] Phenanthrene can be formed in a similar way, through several rearrangements of a recombination product of indenyl and cyclopentadienyl radicals.[25] According to various computational studies of PESs corresponding to these reaction sequences[23,24,26] and recent kinetic studies of propargyl recombination,[27−29] the five-membered ring aromatics (fulvene, cyclopentadiene, and cyclopentadienyl) represent important PAH precursors. In the recent ab initio/QRRK/kinetic modeling study by Richter and Howard,[30] the self-combination of propargyl radicals followed by ring closure and subsequent rearrangements was again shown to be the dominant benzene formation pathway in acetylene and ethylene flames.

The third mechanism of PAH synthesis discussed in the literature can be described as a Diels−Alder-type mechanism, which does not involve radical species during the growth process. It has been proposed by Siegmann and Sattler[31] as the dominant route of PAH growth in methane combustion. In this mechanism, the acetylene molecule acts as a dienophil and effectively closes bay regions in such PAHs as biphenyl, phenanthrene, and so forth. The mechanism (often called a benzogenic Diels−Alder reaction) involves two stages, cycloaddition of C_2H_2 to produce a Diels−Alder adduct, which then undergoes H_2 loss leading to a higher PAH. According to Siegmann and Sattler,[31] this mechanism is favored over the conventional HACA process because it can explain the successive formation of more compact, peri-condensed PAHs observed in methane combustion.

In the present study, we report chemically accurate ab initio G3-type calculations of PESs for possible HACA routes leading from benzene to naphthalene as well as HACA and Diels−Alder routes leading from naphthalene to acenaphthalene. These calculations allow us, for the first time, to consider the HACA network as a whole using most reliable surfaces, which are expected to be accurate within 1−2 kcal/mol. The results of the ab initio calculations, that is, the energies and molecular parameters obtained from the first principles, are utilized in RRKM and TST calculations of reaction rate constants, which are compared with experimental and earlier theoretical data wherever available. Although G3 model chemistry is becoming a standard method for highly accurate predictions of relative energies of intermediates and transition states of chemical reactions, it is conventionally applied to relatively small systems. The applications to larger molecules are scarce so far because of the large computational demands of G3 methods, and systems containing more than 6−7 heavy atoms are most often treated in the literature using much less expensive density functional methods. These methods, unfortunately, are so far unable to provide an accuracy and reliability comparable with those of the G3 family. The accurate energetics are especially important when they are used for the quantitative prediction

of reaction rate constants. Therefore, an additional goal of the present paper is to compare the reaction energies and barrier heights computed by G3 and DFT methods for various types of processes involved in the PAH growth mechanism.

2. Computational Methods

Geometries and vibrational frequencies of all species involved in various reactions were obtained using the hybrid density functional B3LYP[32a−d] method with the 6-311+G(3df,2p) basis set for the HACA naphthalene formation network and the 6-311G** basis set for other reactions, unless mentioned otherwise. Unscaled vibrational frequencies were used to calculate zero-point energy (ZPE) corrections, to characterize the stationary points, and to perform rate constant computations. Although B3LYP as well as other conventional density functionals were shown to produce less accurate results in kinetic calculations than recently developed hybrid DFT methods such as KMLYP,[32e] we used B3LYP instead of those DFT alternatives because the final energies utilized in our kinetics calculations were obtained at a G3-type level, which is considerably more accurate than any available DFT scheme. The differences in calculated frequencies and geometries produced by B3LYP and KMLYP methods differ only slightly, but just the B3LYP method was used in the calibration of several schemes in the G3 family. The optimized geometries of all species (in Cartesian coordinates) involved in the reaction networks, vibrational frequencies, ZPE corrections, and molecular structural parameters (symmetry groups, moments of inertia, and rotational constants) are given in Table S1 of the Supporting Information.

To obtain accurate barrier heights and heats of reactions, we applied the G3 theory[33] for high-level single-point energy calculations. G3 model chemistry has been shown to be less computationally demanding and more accurate than its predecessors, G2 and G2M. We employed the G3(MP2,CC)//B3LYP modification[34] of the original G3 scheme. The final energies at 0 K were obtained using the B3LYP structures, frequencies, and ZPE corrections according to the following formula:

$$E_0[\mathrm{G3(MP2,CC)}] = E[\mathrm{CCSD(T)/6\text{-}31G(d)}] + \Delta E_{\mathrm{MP2}} + \Delta E(\mathrm{SO}) + E(\mathrm{HLC}) + E(\mathrm{ZPE})$$

where ΔE_{MP2} is the basis set correction,

$$\Delta E_{\mathrm{MP2}} = E[\mathrm{MP2/G3MP2large}] - E[\mathrm{MP2/6\text{-}31G(d)}],$$

ΔE(SO) is a spin−orbit correction (significant only for atoms and not included in our calculations), E(HLC) is a high-level correction, and E(ZPE) is the zero-point energy. To further improve the accuracy for reaction species relevant to HACA naphthalene synthesis, we used the 6-311G** and G3large[35] basis sets instead of the 6-31G* and G3MP2large sets,[35] respectively, in the CCSD(T) and MP2 calculations. Here and below, we denote this G3-type scheme applied in our computations as G3 for brevity.

For hydrogen disproportionation steps, which proceed via open-shell singlet transition states, we employed the IRCMax method[36a] where barrier heights were determined as Max{Energy[G3(MP2,CC)]}//IRC{Geom[UMP2/6-31G*]}. The transition state geometries were initially optimized at the UMP2/6-31G* level,[37] then the minimal energy reaction path (MEP) was obtained by intrinsic reaction coordinate (IRC) calculations[38] and energies of the structures along MEP were refined at G3(MP2,CC). We preferred UMP2 geometry optimization over B3LYP in this case because, using the B3LYP method, we were unable to achieve convergence during the saddle-point search on the open-shell singlet PES. It should be noted that the shapes of potential energy curves along MEP appeared to be similar at the UMP2 and G3(MP2,CC) levels, although the exact positions of the transition states and barriers calculated using G3(MP2,CC)//UMP2 and IRCMax differ. Although a more accurate and reliable procedure (VTST-IOC) has been proposed by Chuang et al.[36b] for the reaction path dynamics calculations, we were unable to utilize this scheme for our system because it is significantly more computationally demanding than IRCMax and requires higher-level corrections to energies, frequencies, and moments of inertia, based on stationary-point geometries reoptimized at a higher level than the reaction path calculations. Instead, we utilized the IRCMax scheme considering that it produces more accurate results comparatively with simple MP2 optimization (gradient calculations and frequencies at the G3 level are unavailable so far).

All ab initio calculations were carried out using the Gaussian 98[39] and Molpro 2002[40] program packages. The calculated heats of reactions and barrier heights are summarized in Table 1.

High-pressure thermal rate constants were computed using the RRKM[41−43] theory and conventional TST.[44] The latter was applied for hydrogen abstraction/disproportionation steps, which are bimolecular in both forward and backward directions. Tunneling corrections (Q_{tun}) to the rate constants were calculated using simple Wigner's formula[41] because at combustion temperatures (>1000 K), tunneling does not play a significant role and more sophisticated estimates for tunneling corrections are not necessary.

For unimolecular steps, we carried out conventional RRKM calculations utilizing the energetic and molecular parameters (reaction barriers, moments of inertia, vibrational frequencies) from the ab initio calculations. RRKM rate constants obtained in the present study correspond to the high-pressure limit reaction conditions. The modified Beyer−Swinehart algorithm[45,46] was employed in calculations of the numbers and densities of states. For some intermediates and transition states, which exhibit low-frequency torsional motions, we applied the free internal rotor approximation[41−43] to evaluate their contributions to the partition functions. Such low-frequency modes usually correspond to internal rotations with barriers substantially below $k_{\mathrm{B}}T$, which cannot be properly described by a harmonic oscillator. It should be noted that the free-rotor treatment provides upper estimates for contributions of torsional motions to the partition function. In the free internal rotor calculations, we obtained moments of inertia associated with the free rotor as reduced moments of inertia of two fragments rotating around a single torsional axis.

Table 1. Barrier Heights and Reaction Energies for All Steps Involved in the Studied PAH Formation Mechanisms Computed at the G3(MP2,CC) and B3LYP[a] Levels

		barrier height, kcal/mol		reaction energy, kcal/mol	
raection	TS	G3(MP2,CC)	B3LYP	G3(MP2,CC)	B3LYP
		Hydrogen Abstraction			
A1 + H → A2 + H_2	TS1a	16.5 (17.0)[b]	10.8	8.5 (8.8)[b]	5.2
A1 + OH → A2 + H_2O	TS1b	5.5	0.42	−5.4	−5.5
N1 + OH → N2 + H_2O	TS1a^{AN}	6.3	−1.0[c]	−3.4	−2.4[c]
A1 + CH_3 → A2 + CH_4	TS1c	17.8	15.8	8.8	7.5
A7 + H → A6 + H_2	TS8	17.6	11.5	8.5	4.5
A10 + H → A11 + H_2	TS13	17.9	11.9	10.2	6.3
N1 + H → N2 + H_2	TS1^{AN}	17.5	11.1[c]	9.7	5.6[c]
		Acetylene Addition			
A2 + C_2H_2 → A3	TS2	3.5	4.6	−39.2	−36.9
N2 + C_2H_2 → N3	TS2^{AN}	2.3	4.1[c]	−39.6	−37.0[c]
A3 + C_2H_2 → A4	TS3	4.8	5.2	−39.5	−39.3
A3a + C_2H_2 → A4b	TS7b	5.5	6.8	−32.7	−32.2
A6 + C_2H_2 → A8	TS9	3.9	6.2	−37.6	−33.4
A11 + C_2H_2 → A12	TS14	1.9	3.6	−40.8	−37.9
		Ring Closure (Radical Cyclization)			
A4b → A5	TS5	3.6	4.6	−32.3	−29.3
A8 → A9	TS10	1.8	2.2	−47.6	−49.0
A12 → A13	TS15	5.4	4.8	−53.1	−53.8
N3 → N4	TS3^{AN}	16.6	16.2[c]	−19.9	−16.1[c]
		Hydrogen Atom Loss/Disproportionation			
A3 → A10 + H	TS12	36.6	37.8	30.1	33.3
A5 → N1 + H	TS6	14.8	14.2	2.5	5.2
A9 → N1 + H	TS11	27.8	28.1	21.2	24.8
N4 → AN + H	TS4^{AN}	26.3	27.8[c]	19.2	23.1[c]
A3 + H → A10 + H_2	TS12a	12.0 (6.2)[d]		−74.2[e]	
A5 + H → N1 + H_2	TS6a	2.7 (1.2)[d]		−101.7[e]	
A9 + H → N1 + H_2	TS11a	5.0 (2.3)[d]		−82.5[e]	
N4 + H → AN + H_2	TS4a^{AN}	10.6 (5.3)[d]		−84.5[e]	
		Acetylene Cycloaddition/H_2 Loss (Diels−Alder Mechanism)			
N1 + C_2H_2 → N5	TS5^{AN}	66.3	72.4[c]	47.6	58.0[c]
B1 + C_2H_2 → B2	TS1^{P}	42.2	48.3[c]	3.57	13.4[c]
P + C_2H_2 → P1	TS1^{PYR}	42.0	48.2[c]	4.78	14.6[c]
N5 → AN + H_2	TS6^{AN}	24.2	24.0[c]	−76.8	−82.4[c]
B2 → P + H_2	TS2^{P}	17.9	15.7[c]	−53.9	−60.0[c]
P1 → PYR + H_2	TS2^{PYR}	18.3	16.9[c]	−56.6	−62.5[c]
		Hydrogen Migration/Isomerization			
A3a → A6	TS7	27.6	27.7	1.5	1.2
A3 → A3a	TS7a	2.9	2.2	−1.0	−1.1
A4 → A4a	TS4	4.2	6.4	2.4	3.2
A4a → A4b	TS4a	73.0	37.6	3.3	2.8
		Hydrogen Atom Addition (Radical Recombination)			
A3a + H → A7				−108.1	−107.2
A13 + H → N1				−111.0	−109.3

[a] B3LYP energies correspond to the B3LYP/6-311+G(3df,2p) calculations if not mentioned otherwise. [b] Computed at the G3(CC)//B3LYP and G3(MP2,CC)//B3LYP (in parentheses) levels. [c] Computed at the B3LYP/6-311G** level. [d] Computed at the IRCMax{Energy[G3(MP2,CC)]}// IRC{Geom[UMP2/6-31G*]} and G3(MP2,CC)//UMP2/6-31G* (in parentheses) levels. [e] Computed at the G3(MP2,CC)//MP2/6-31G* level.

All RRKM- and TST-computed rate constants in the form of fitted modified Arrhenius rate expressions $k = AT^n \exp(-E/RT)$ are presented in Table S2 of the Supporting Information. Individual rate constants at temperatures of 1000−3000 K are shown in Table 2.

3. Potential Energy Surfaces and Reaction Rate Constants

Various reaction pathways involved in the HACA and Diels−Alder syntheses of naphthalene and acenaphthalene and also of phenanthrene and pyrene are shown in Figure 1 along with chosen notations for all species and transition states. The A3a → A4b → A5 → N1 and A3 → A4 → A4a → A4b → A5 → N1 branches represent Bittner−Howard's route, whereas the A3 → A10 → A11 → A12 → A13 → N1 sequence represents Frenklach's mechanism of HACA naphthalene synthesis. The A3a → A6(A7) → A8 → A9 → N1 branch is a variation of Frenklach's mechanism, where the second acetylene adds to the aromatic ring of the 1-vinyl-2-phenyl radical (A6) after its prior activation either by conventional (A7 → A6) or internal (A3a → A6) hydrogen abstraction. The N1 → N2 → N3 → N4 → AN and N1 → N5 → AN reaction sequences represent the HACA and Diels−Alder routes, respectively, leading from naphthalene to the acenaphthalene. The other two Diels−Alder routes lead from biphenyl to phenanthrene (B1 → B2 → P) and from phenanthrene to pyrene (P → P1 → PYR).

In subsequent sections, we discuss the results of our ab initio G3-type calculations of PESs for all relevant reaction steps and RRKM/TST computed rate coefficients. We also compare calculated barrier heights and reaction energies with available-in-the-literature experimental activation energies and heats of reactions, respectively. Although phenomenological activation energies normally obtained from the temperature dependence (Arrhenius plots) of measured rate constants often exhibit a complex character, we suppose, on the basis of activated complex theory, that theoretically derived barriers are closely related to them if both correspond

Table 2. Calculated Rate Constants (in Units of s^{-1} and $cm^3\ s^{-1}\ mol^{-1}$ for Unimolecular and Bimolecular Steps, Respectively)

reaction	rate constant	temperature, K				
		1000	1500	2000	2500	3000
Naphthalene Formation Network						
A1 + H → A2 + H_2	k_{TS1}	6.96×10^{10}	1.92×10^{12}	1.18×10^{13}	3.87×10^{13}	9.07×10^{13}
A2 + H_2 → A1 + H	k_{TS-1}	8.1×10^{10}	5.41×10^{11}	1.71×10^{12}	3.86×10^{12}	7.19×10^{12}
A2 + C_2H_2 → A3	k_{TS2}	1.0×10^{12}	3.81×10^{12}	8.86×10^{12}	1.63×10^{13}	2.62×10^{13}
A3 → A2 + C_2H_2	k_{TS-2}	6.37×10^{5}	1.03×10^{9}	4.17×10^{10}	3.83×10^{11}	1.68×10^{12}
A3 → A10 + H	k_{TS12}	6.62×10^{5}	4.93×10^{8}	1.47×10^{10}	1.18×10^{11}	4.92×10^{11}
A10 + H → A3	k_{TS-12}	2.76×10^{12}	1.27×10^{13}	3.09×10^{13}	5.71×10^{13}	9.04×10^{13}
A3 + H → A10 + H_2	k_{TS12a}	2.92×10^{10}	1.96×10^{11}	5.30×10^{11}	9.85×10^{11}	1.51×10^{12}
A10 + H_2 → A3 + H	k_{TS-12a}	4.21×10^{-6}	8.23	1.29×10^{4}	1.14×10^{6}	2.35×10^{7}
A10 + H → A11 + H_2	k_{TS13}	1.24×10^{10}	4.47×10^{11}	3.15×10^{12}	1.12×10^{13}	2.77×10^{13}
A11 + H_2 → A10 + H	k_{TS-13}	8.85×10^{10}	5.76×10^{11}	1.8×10^{12}	4.02×10^{12}	7.45×10^{12}
A11 + C_2H_2 → A12	k_{TS14}	2.27×10^{11}	7.69×10^{11}	1.75×10^{12}	3.25×10^{12}	5.34×10^{12}
A12 → A11 + C_2H_2	k_{TS-14}	3.42×10^{5}	6.48×10^{8}	2.92×10^{10}	2.93×10^{11}	1.38×10^{12}
A12 → A13	k_{TS15}	1.01×10^{11}	2.45×10^{11}	3.83×10^{11}	5.01×10^{11}	6.0×10^{11}
A13 → A12	k_{TS-15}	33.8	1.01×10^{6}	1.86×10^{8}	4.42×10^{9}	3.74×10^{10}
A3 → A3a	k_{TS7a}	2.38×10^{12}	4.39×10^{12}	6.08×10^{12}	7.49×10^{12}	8.67×10^{12}
A3a → A3	k_{TS-7a}	2.07×10^{12}	4.52×10^{12}	6.81×10^{12}	8.82×10^{12}	1.06×10^{13}
A3a → A6	k_{TS7}	4.49×10^{6}	4.66×10^{8}	4.98×10^{9}	2.12×10^{10}	5.66×10^{10}
A6 → A3a	k_{TS-7}	1.06×10^{7}	9.01×10^{8}	8.8×10^{9}	3.58×10^{10}	9.33×10^{10}
A6 + C_2H_2 → A8	k_{TS9}	2.82×10^{10}	1.32×10^{11}	3.54×10^{11}	7.29×10^{11}	1.28×10^{12}
A8 → A6 + C_2H_2	k_{TS-9}	2.95×10^{5}	4.61×10^{8}	1.9×10^{10}	1.81×10^{11}	8.25×10^{11}
A8 → A9	k_{TS10}	2.72×10^{12}	3.91×10^{12}	4.71×10^{12}	5.29×10^{12}	5.72×10^{12}
A9 → A8	k_{TS-10}	4.81×10^{3}	2.84×10^{7}	2.26×10^{9}	3.2×10^{10}	1.9×10^{11}
A9 → N1 + H	k_{TS11}	1.96×10^{7}	2.99×10^{9}	3.98×10^{10}	1.96×10^{11}	5.86×10^{11}
N1 + H → A9	k_{TS-11}	2.29×10^{12}	1.07×10^{13}	2.62×10^{13}	4.86×10^{13}	7.71×10^{13}
A9 + H → N1 + H_2	k_{TS11a}	2.16×10^{11}	6.18×10^{11}	1.16×10^{12}	1.81×10^{12}	2.53×10^{12}
N1 + H_2 → A9 + H	k_{TS-11a}	1.20×10^{-6}	4.46	1.04×10^{4}	1.22×10^{6}	3.14×10^{7}
A3a + C_2H_2 → A4b	k_{TS7b}	5.67×10^{10}	2.85×10^{11}	7.56×10^{11}	1.5×10^{12}	2.53×10^{12}
A4b → A3a + C_2H_2	k_{TS-7b}	1.99×10^{6}	1.98×10^{9}	6.64×10^{10}	5.65×10^{11}	2.41×10^{12}
A4b → A5	k_{TS5}	3.99×10^{10}	9.13×10^{10}	1.45×10^{11}	1.98×10^{11}	2.48×10^{11}
A5 → A4b	k_{TS-5}	5.97×10^{5}	3.22×10^{8}	7.65×10^{9}	5.2×10^{10}	1.88×10^{11}
A5 → N1 + H	k_{TS6}	9.1×10^{9}	1.4×10^{11}	5.87×10^{11}	1.44×10^{12}	2.69×10^{12}
N1 + H → A5	k_{TS-6}	8.94×10^{10}	9.92×10^{11}	3.77×10^{12}	9.07×10^{12}	1.72×10^{13}
A5 + H → N1 + H_2	k_{TS6a}	1.40×10^{12}	3.01×10^{12}	4.82×10^{12}	6.76×10^{12}	8.78×10^{12}
N1 + H_2 → A5 + H	k_{TS-6a}	5.13×10^{-10}	3.68×10^{-2}	3.73×10^{2}	1.01×10^{5}	4.89×10^{6}
Acenaphthalene Formation Network						
N1 + H → N2 + H_2	k_{TS1}^{AN}	2.86×10^{10}	9.45×10^{11}	6.37×10^{12}	2.2×10^{13}	5.35×10^{13}
N2 + H_2 → N1 + H	k_{TS-1}^{AN}	8.30×10^{10}	5.44×10^{11}	1.7×10^{12}	3.81×10^{12}	7.07×10^{12}
N2 + C_2H_2 → N3	k_{TS2}^{AN}	6.97×10^{11}	2.18×10^{12}	4.58×10^{12}	7.94×10^{12}	1.23×10^{13}
N3 → N2 + C_2H_2	k_{TS-2}^{AN}	1.83×10^{6}	2.61×10^{9}	9.84×10^{10}	8.7×10^{11}	3.72×10^{12}
N3 → N4	k_{TS3}^{AN}	3.77×10^{8}	6.34×10^{9}	2.65×10^{10}	6.32×10^{10}	1.14×10^{11}
N4 → N3	k_{TS-3}^{AN}	2.96×10^{5}	1.71×10^{8}	4.25×10^{9}	2.98×10^{10}	1.1×10^{11}
N4 → AN + H	k_{TS4}^{AN}	6.55×10^{7}	7.85×10^{9}	9.24×10^{10}	4.24×10^{11}	1.2×10^{12}
AN + H → N4	k_{TS-4}^{AN}	8.53×10^{11}	4.27×10^{12}	1.09×10^{13}	2.07×10^{13}	3.35×10^{13}
N4 + H → AN + H_2	k_{TS4a}^{AN}	1.09×10^{10}	7.55×10^{10}	2.16×10^{11}	4.27×10^{11}	6.95×10^{11}
AN + H_2 → N4 + H	k_{TS-4a}^{AN}	6.80×10^{-9}	8.41×10^{-2}	3.50×10^{2}	5.75×10^{4}	1.84×10^{6}
N1 + C_2H_2 → N5	k_{TS5}^{AN}	2.29×10^{-4}	34.5	1.68×10^{4}	7.87×10^{5}	1.12×10^{7}
N5 → N1 + C_2H_2	k_{TS-5}^{AN}	4.42×10^{9}	1.26×10^{11}	6.91×10^{11}	1.94×10^{12}	3.89×10^{12}
N5 → AN + H_2	k_{TS6}^{AN}	2.86×10^{7}	1.85×10^{9}	1.59×10^{10}	6.01×10^{10}	1.5×10^{11}
AN + H_2 → N5	k_{TS-6}^{AN}	2.29×10^{-10}	8.08×10^{-3}	59.5	1.41×10^{4}	5.88×10^{5}

to a one-step mechanism, and therefore, they can be directly compared. Most of the reactions considered here are indeed dominated by one-step mechanisms (with few exceptions mentioned in the discussion, such as, for example, the C_6H_5 + OH reaction). The calculated rate constants are further scrutinized by a comparison of their absolute values and temperature dependence with those for experimental rate coefficients.

All networks studied here involve several types of reactions. The HACA mechanism includes hydrogen abstractions (we considered H-abstractions by H, OH, and CH_3 radicals), acetylene additions to the radical site, ring closures, and hydrogen atom loss/disproportionation reactions. Only two reaction steps are involved in the Diels−Alder mechanism, acetylene cycloaddition to a singlet PAH molecule and H_2 elimination from the Diels−Alder adduct. Below, we sequentially discuss these reaction types in more detail.

3.1. Hydrogen Abstraction Steps. A. Ab Initio Calculations. The H atom abstraction from a singlet PAH species can occur through its reactions with H/OH radicals ubiquitous in flames or by the reactions with small hydrocarbon radicals, for example, CH_3, C_2H_5, and so forth. Here, we consider the H-abstraction reactions of benzene (A1) with H, OH, and CH_3 and of naphthalene (N1) with H and OH radicals. For the other H-abstraction steps, we limited our consideration to the reactions with H radicals. The mechanism and kinetics of H abstraction from benzene, C_6H_6 + H, have been studied experimentally employing different techniques[47−49] and theoretically using ab initio G2M(rcc,MP2) calculations and the TST method.[16] Several experimental and theoretical kinetic studies on the C_6H_6 + OH abstraction[50−55] provided a large amount of data for comparison with theoretical results. Recently, this reaction was thoroughly investigated by Tokmakov and Lin[17] using G3 and G2M model chemistry methods in conjunction with the weak collision master equation/RRKM analysis. The kinetics of the C_6H_6 + CH_3 abstraction reaction were studied experimentally by Krech and Price[56] and Zhang et al.[57] Most recently, this reaction

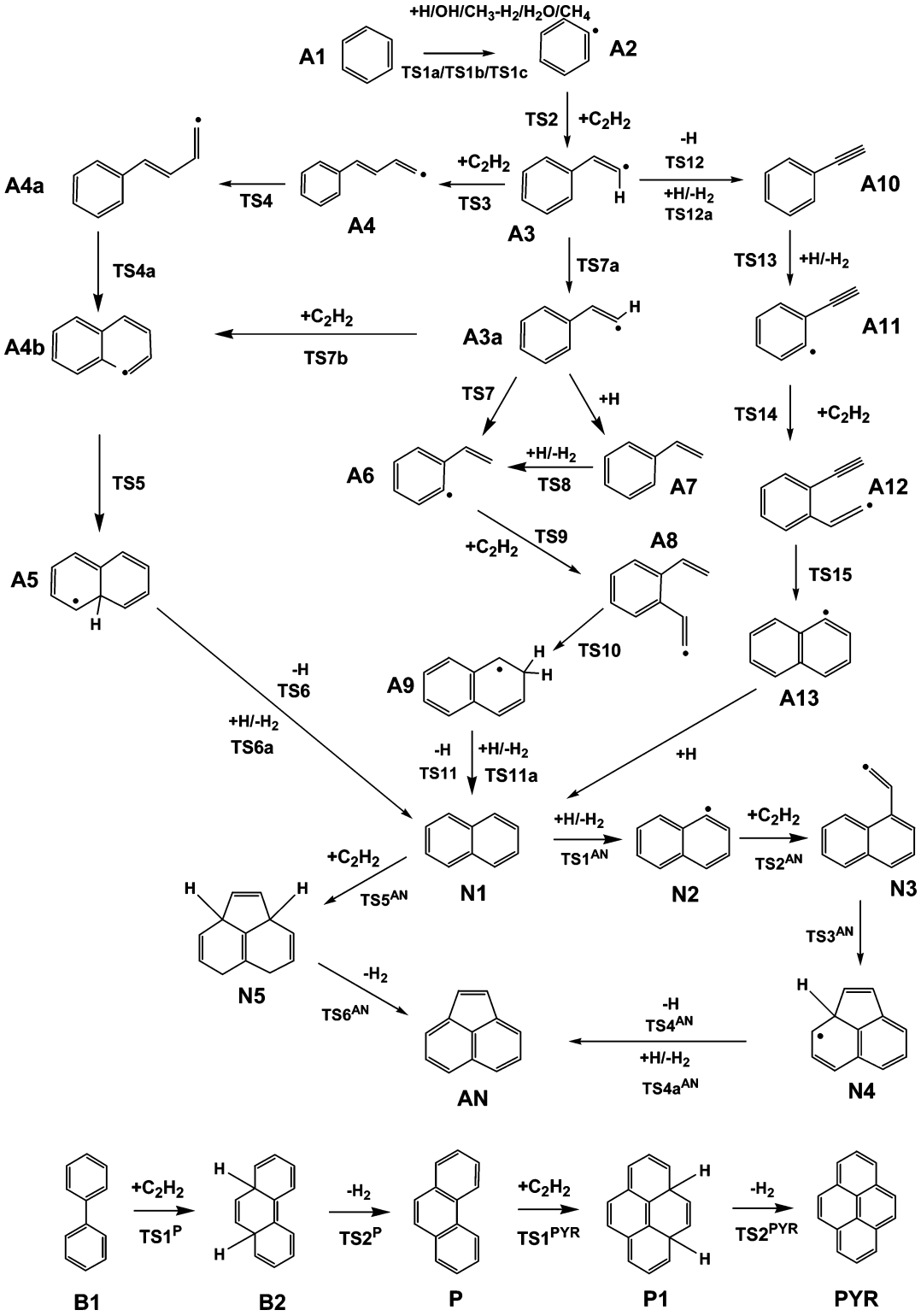

Figure 1. Various reaction pathways involved in the HACA synthesis of naphthalene and acenaphthalene and the Diels−Alder synthesis of acenaphthalene, phenanthrene, and pyrene.

was analyzed both theoretically and experimentally by Tokmakov et al.,[19] who applied two complementary experimental methods, pyrolysis/Fourier transform infrared spectroscopy, and pulsed laser photolysis/mass spectrometry, as well as theoretical G2M(CC,MP2) calculations. For the H-abstraction from naphthalene (N1 → N2), no accurate experimental/theoretical data are available in the literature.

Let us first consider the A1 → A2, A7 → A6, A10 → A11, and N1 → N2 steps, where the abstraction of a H atom from singlet PAH intermediates occurs by the H radical. Because the H-abstraction reactions are endothermic by 8.8−10.2 kcal/mol (see Table 1), all transition states exhibit a late, product-like character. The calculated reaction energies and barrier heights are very similar; the differences between

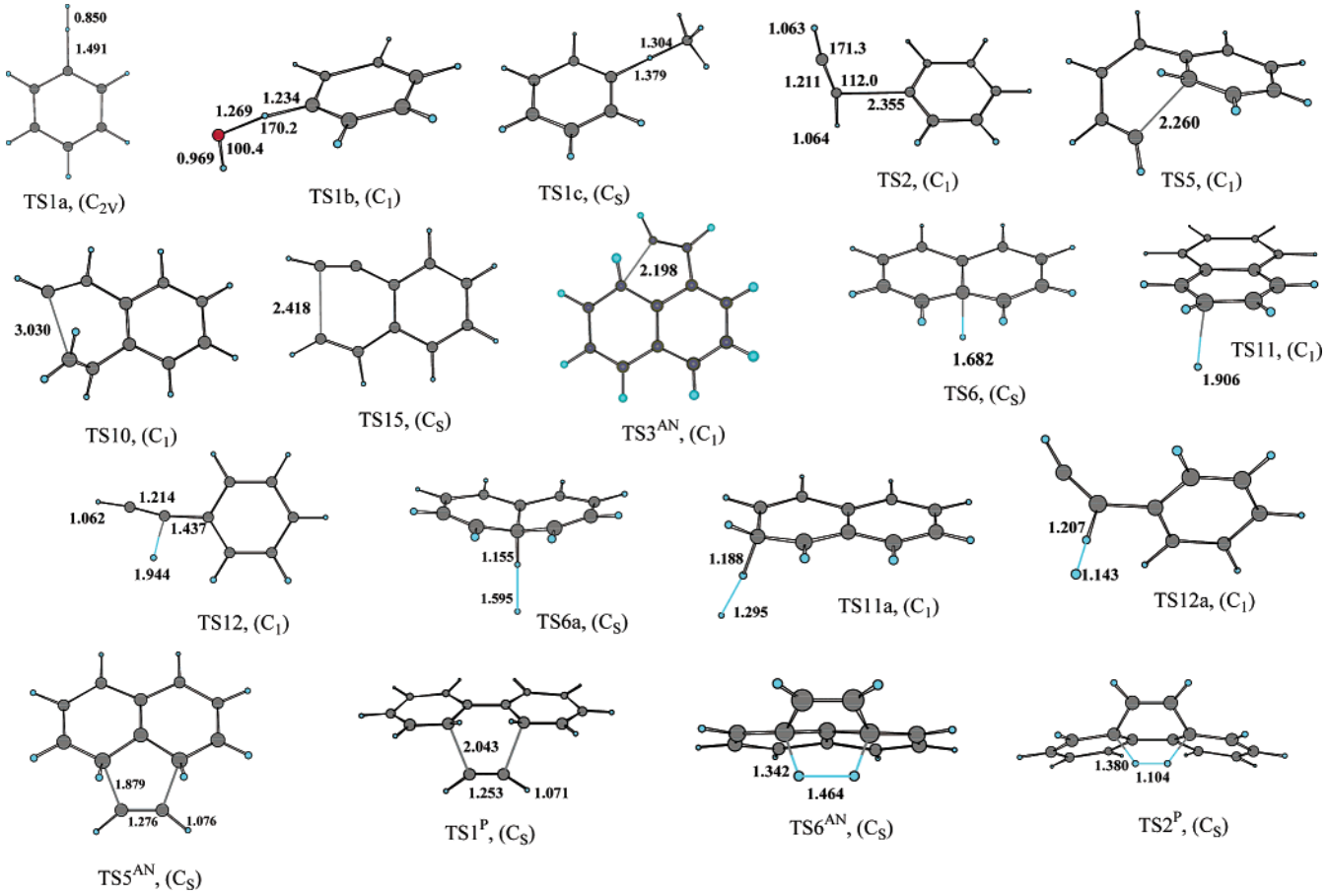

Figure 2. Optimized geometries of various transition states. Selected bond lengths are shown in Å. (For full optimized geometries, see Table S1 in the Supporting Information.)

different reactions do not exceed 1.5 kcal/mol. The highest barrier (17.9 kcal/mol) and heat of reaction (10.2 kcal/mol) are found for the H abstraction from A10 (phenylacetylene), while the lowest barrier (16.5 kcal/mol) is computed for C_6H_6 + H. As seen in Table 1, the B3LYP method significantly underestimates barriers and heats of reaction for the hydrogen-abstraction steps. For example, the B3LYP calculated barrier and heat of the C_6H_6 + H abstraction are found to be 5.7 and 3.3 kcal/mol lower, respectively, than the respective values obtained at the G3 level. The G3 computed barrier height of 16.5 kcal/mol for C_6H_6 + H closely agrees with the experimental activation energy of 16.0 kcal/mol derived from the Arrhenius expression $k(T) = 4.15 \times 10^{-10} \exp[-16\,000/RT]$ cm^3 molecule^{-1} s^{-1} obtained by Kiefer et al.[49] in the high-temperature shock tube pyrolysis of benzene in the temperature range $T = 1900-2200$ K. Similarly close agreement is also found for the heat of reaction, 8.7 ± 0.6 kcal/mol[16] from the experiment and 8.5 kcal/mol at the G3 level. The G2M(rcc,MP2) calculated barrier height and reaction energy for this abstraction step, 19.9 and 11.1 kcal/mol, respectively,[16] are notably higher than the experimental and G3 values. Thus, G3 theory, in this case, provides more accurate energetics than G2M, which tends to overestimate both the barrier and heat of the reaction.

H abstractions by a hydroxyl radical from benzene (A1 + OH) and naphthalene (N1 + OH) exhibit significantly lower barriers (5−6 kcal/mol) than the abstractions by a H radical and are slightly exothermic (by 3−5 kcal/mol). As a result, the structures of corresponding transition states TS1b and $TS1b^{AN}$ exhibit an early character (see Figure 2). As seen in Table S1 of the Supporting Information, TS1b and $TS1b^{AN}$ have low-frequency vibrational modes (lower or about 100 cm^{-1}) corresponding to a torsional motion of the OH group.

Interestingly, the barrier is higher and the exothermicity is lower for the H abstraction by OH from naphthalene than those from benzene. A comparison of B3LYP and G3 barriers and reaction energies for these reactions (Table 1) shows that the B3LYP method significantly underestimates the barrier for the C_6H_6 + OH abstraction, giving an unreasonably low value of 0.4 kcal/mol. For the N1 + OH abstraction, the B3LYP method fails and predicts a negative reaction barrier, which could be caused by the use of a smaller 6-311G** basis set as compared to 6-311+G(3df,-2p) employed for C_6H_6 + OH. The agreement between B3LYP and G3 is good for the heats of reaction, especially, for the C_6H_6 + OH abstraction. While comparing the G3 calculated barrier heights with experimental and theoretical activation energies,[50−55] we have to keep in mind the possibility of the second competitive nonabstraction channel, PAH + OH → PAH−OH, which can contribute to the overall reaction rate and affect the energetic parameters derived from Arrhenius expressions. In some earlier studies,[58,59] the OH addition was recognized as the main reaction channel. However, according to the experimental study by Madronich and Felder,[51] the OH addition channel does not

contribute significantly (<20%) to the overall reaction rate at temperatures relevant to combustion (T > 1000 K). The experimental activation energy of the C_6H_6 + OH abstraction derived in that work is 4.8 kcal/mol, close to our G3-type result of 5.5 kcal/mol and to the G3 value of 5.3 kcal/mol reported by Tokmakov and Lin.[17] Other experimental kinetic measurements for the C_6H_6 + OH reaction[50,52−54] gave different estimates for the activation energy varying from 3.7 to 5.6 kcal/mol. Taking into account the relatively low activation energy and the fact that these experimental works were carried out at different times, using different techniques and temperature ranges, and that they must have different systematic errors, the agreement with the theoretical barrier heights is quite satisfactory. For the reaction energy, our value of −5.4 kcal/mol is very close to the experimental estimate[17] of −5.6 ± 0.8 kcal/mol obtained using thermodynamic parameters from standard reference sources.

Because the H abstraction from benzene by a methyl radical, C_6H_6 + CH_3, was recently studied using the G2M(CC,MP2) method,[19] here we only briefly compare our G3 results with the previous literature data and with the corresponding parameters for the C_6H_6 + H reaction obtained at the same level of theory. The G3 computed reaction barrier of 17.8 kcal/mol and endothermicity of 8.8 kcal/mol for C_6H_6 + CH_3 are close to those for the H abstraction by a H radical, 16.5 and 8.5 kcal/mol, respectively. The transition state TS1c exhibits the same loose, product-like character as that of TS1a for C_6H_6 + H (Figure 2). A specific feature of TS1c is the presence of a very low-frequency mode of 16 cm^{-1} (see Table S1, Supporting Information) corresponding to the internal rotation of the methyl group and two other nearly degenerate modes (86 and 90 cm^{-1}) assigned to bending vibrations of the C−H−C fragment in and out of the symmetry plane. The possibility of the quasi-free methyl rotation makes PESs in the vicinity of TS1c very flat; our B3LYP/6-311+G(3df,2p) optimization gave a C_s-symmetric structure for the transition state, whereas Tokmakov et al.[19] obtained a C_1 structure with a smaller basis set. The difference is, however, insignificant because the energies of the two structures differ only by 0.01 kcal/mol.

The agreement of our G3 computed reaction endothermicity (8.8 kcal/mol) with that of the experiment (8.8 ± 0.9 kcal/mol)[19] is excellent and better than that for the G2M(CC,MP2) value of 10.3 kcal/mol.[19] For the reaction barrier, our value of 17.8 kcal/mol is 1.8 kcal/mol lower than the 19.6 kcal/mol obtained by Tokmakov et al.[19] From the Arrhenius expressions, $k(T) = 6.3 \times 10^{10} \exp[-4680/T]$ cm^3 mol^{-1} s^{-1} by Krech and Price[56] and $k(T) = 2.0 \times 10^{12} \exp[-7580/T]$ cm^3 mol^{-1} s^{-1} by Zhang et al.[57] obtained in early experiments, the activation energies for the C_6H_6 + CH_3 reaction are estimated as 9.7 and 15.8 kcal/mol, both significantly lower than the theoretical predictions. Tokmakov et al.[19] concluded that the kinetic data reported in these works are not reliable and are inconsistent with the higher barrier predicted by accurate ab initio calculations. It is known[16,19] that the G2M method systematically overestimates barrier heights for the C_6H_6 + H and C_6H_6 + CH_3 abstraction reactions because of the unbalanced accuracy of the calculated energies for the reactants and products. To avoid this, the barriers can be corrected for the error in the enthalpy of the reaction. Using such corrections, the G2M values of 19.6 and 19.9[16] kcal/mol for the barrier heights of the C_6H_6 + CH_3 and C_6H_6 + H reactions can be reduced to the values of 18.1 kcal/mol[19] and 17.5 kcal/mol, respectively, which are closer to our G3 results of 17.8 and 16.5 kcal/mol. We conclude again from this comparison that the G3 method could produce highly accurate barriers and enthalpies for H abstraction and, therefore, represents a big improvement for calculations of PESs for these kind of reactions as compared to the G2 theory.

Interestingly, we found a better agreement between G3 and B3LYP calculated barriers and heats of the C_6H_6 + CH_3 reaction than for C_6H_6 + H and similar abstraction reactions by a H radical (N1 + H, A7 + H, and A10 + H). Indeed, for the barrier height for C_6H_6 + CH_3, the difference between G3 and B3LYP/6-311+G(3df,2p) results is only 2 kcal/mol versus 5.7 kcal/mol for the C_6H_6 + H abstraction. For the reaction endothermicity, this difference is even smaller, 1.3 kcal/mol, compared to the 3.3 kcal/mol difference for C_6H_6 + H. Thus, the B3LYP method should perform better for the abstraction reactions by small hydrocarbon radicals than for those by H/OH radicals. We can attribute this difference to the worse ability of B3LYP to correctly predict the H−H bond energies in TS1a and the H_2 molecule.

3.1.B. Rate Constant Calculations. The bimolecular rate constants for the hydrogen-abstraction steps at three temperatures relevant to combustion, 1000, 1500, and 2000 K, and fitted rate expressions are compared in Table 3 with kinetic data available from the literature. For the C_6H_6 + H reaction, the comparison shows a reasonably good agreement (within a factor of 2.25) between our G3/TST computed rate constants, previous G2M/TST results,[16] and the experimental data of Kiefer et al.[49] obtained in the high-temperature shock tube pyrolysis of benzene. The rate expression $4.15 \times 10^{-10} \exp[-16\,000/RT]$ cm^3 $molecule^{-1}$ s^{-1} suggested by Kiefer et al.[49] is the common expression normally used in kinetic modeling studies for the rate constants of H-atom abstraction from different hydrocarbons (see, for example, ref 60). Nicovich and Ravishankara[48] derived a much lower activation energy of 8.1 kcal/mol in their rate expression suggested for 300−1000 K; however, their absolute rate constant at 1000 K agrees with our theoretical data.

Although the calculated barrier heights for the C_6H_6 + H, N1 + H, A7 + H, and A10 + H reactions differ only slightly, the rate constants for the last three reactions are significantly lower than that for C_6H_6 + H. This difference is especially large (nearly 2 orders of magnitude) for A7 + H at low combustion temperatures ($T \sim 1000$ K). The lower rates for the N1 + H, A7 + H, and A10 + H reactions are due to the lower pre-exponential factors. If we compare rotational symmetry numbers of the reactants, 12 for C_6H_6, 4 for N1, 1 for A7, and 2 for A10, we can see that for benzene, its value is much higher than those for the other species. For the respective transition states, TS1a (2), $TS1^{AN}$ (1), TS8 (1), and TS13 (1), the difference in symmetry numbers is not substantial. The higher value of the rotational symmetry number for benzene significantly affects its partition function and results in a considerable increase of the rate constant

Table 3. Comparison of Available Rate Expressions $k = AT^n \exp(-E/RT)$ and Rate Constants at Several Temperatures Relevant to Combustion for Various HACA and Diels−Alder Steps

	rate expressions			rate constants[a] at T =					
reaction	A[a]	n	E, cal/mol	1000 K	1500 K	2000 K	temperature range, K	method	reference
Hydrogen Abstraction									
A1 + H → A2 + H_2	6.44×10^{-16}	1.86	15 976	1.16×10^{-13}	3.23×10^{-12}	1.99×10^{-11}	300−3000	G3	this work
A1 + H → A2 + H_2	1.00×10^{-15}	1.80	17 107	6.70×10^{-14}	2.16×10^{-12}	1.43×10^{-11}	300−5000	G2M	16
A1 + H → A2 + H_2	4.15×10^{-10}	0	16 000	1.88×10^{-13}	2.45×10^{-12}	8.84×10^{-12}	1900−2200	exp.	49
A1 + H → A2 + H_2	5.00×10^{-12}	0	8100	1.02×10^{-13}	3.72×10^{-13}	7.12×10^{-13}	300−1000	exp.	48
N1 + H → N2 + H_2	4.41×10^{-16}	1.87	17 097	4.74×10^{-14}	1.59×10^{-12}	1.07×10^{-11}	300−3000	G3	this work
A7 + H → A6 + H2	8.68×10^{-19}	2.36	16 917	2.95×10^{-15}	1.17×10^{-13}	8.93×10^{-13}	300−3000	G3[b]	this work
A7 + H → A6 + H2				3.99×10^{-15}	1.30×10^{-13}	8.61×10^{-13}	300−3000	G3	this work
A10 + H → A11 + H_2	2.14×10^{-16}	1.89	17 580	2.06×10^{-14}	7.53×10^{-13}	5.30×10^{-12}	300−3000	G3	this work
A1 + OH → A2 + H_2O	8.62×10^{-21}	3.04	3675	1.93×10^{-12}	1.22×10^{-11}	3.93×10^{-11}	300−3000	G3	this work
A1 + OH → A2 + H_2O	6.70×10^{-22}	3.33	1522	3.15×10^{-12}	1.55×10^{-11}	4.57×10^{-11}	200−2500	G3	17
A1 + OH → A2 + H_2O	3.50×10^{-11}	0	4781	3.51×10^{-12}	7.55×10^{-12}	1.11×10^{-11}	790−1410	exp.	51
A1 + OH → A2 + H_2O	4.67×10^{-18}	2.0	1129	2.71×10^{-12}	7.32×10^{-12}	1.42×10^{-11}	453−1409	exp.[c]	52
A1 + OH → A2 + H_2O	2.70×10^{-16}	1.42	1522	2.32×10^{-12}	5.28×10^{-12}	8.97×10^{-12}		exp.	53
A1 + OH → A2 + H_2O	3.10×10^{-12}	0	5612	2.08×10^{-13}	5.12×10^{-13}	8.04×10^{-13}	213−1150	exp.	50
N1 + OH → N2 + H_2O	1.60×10^{-21}	3.02	4374	2.16×10^{-13}	1.51×10^{-12}	5.12×10^{-12}	300−3000	G3	this work
N1 + OH → N2 + H_2O	1.12×10^{-17}	2.0	2014	4.25×10^{-12}	1.32×10^{-11}	2.76×10^{-11}	≥600	exp.[c]	52
N1 + OH → N2 + H_2O	1.05×10^{-12}	0	1875	4.26×10^{-13}	5.75×10^{-13}	6.69×10^{-13}	≤410	exp.[c]	52
A1 + CH_3 → A2 + CH_4	8.87×10^{-21}	2.89	15 992	1.90×10^{-15}	8.02×10^{-14}	6.72×10^{-13}	300−3000	G3[b]	this work
A1 + CH_3 → A2 + CH_4				2.51×10^{-14}	1.29×10^{-12}	1.25×10^{-11}	300−3000	G3	this work
A1 + CH_3 → A2 + CH_4	2.27×10^{-25}	4.23	14 723	9.32×10^{-16}	5.49×10^{-14}	6.03×10^{-13}	300−2500	G2M[d]	19
A1 + CH_3 → A2 + CH_4	1.05×10^{-13}	0	9728	9.71×10^{-16}	4.62×10^{-15}	1.01×10^{-14}	744−800	exp.	56
A1 + CH_3 → A2 + CH_4	3.32×10^{-12}	0	15 756	1.70×10^{-15}	2.12×10^{-14}	7.50×10^{-14}	650−770	exp.	57
A2 + CH_4 → A1 + CH_3	3.59×10^{-22}	3.22	6948	5.63×10^{-14}	6.47×10^{-13}	2.86×10^{-12}	300−3000	G3[b]	this work
A2 + CH_4 → A1 + CH_3				7.41×10^{-13}	1.04×10^{-11}	5.30×10^{-11}	300−3000	G3	this work
A2 + CH_4 → A1 + CH_3	6.46×10^{-27}	4.57	5498	2.35×10^{-14}	3.62×10^{-13}	2.10×10^{-12}	300−2500	G2M	19
A2 + CH_4 → A1 + CH_3	$10^{12.78}$	0	6201	2.03×10^{-14}	1.60×10^{-13}	4.51×10^{-13}	600−980	exp.	19
Acetylene Addition									
A2 + C_2H_2 → A3	5.46×10^{-18}	2.0484	3162	1.69×10^{-12}	6.40×10^{-12}	1.48×10^{-11}	300−3000	G3[b]	this work
A2 + C_2H_2 → A3				8.52×10^{-13}	3.79×10^{-12}	9.92×10^{-12}	300−3000	G3	this work
A2 + C_2H_2 → A3	2.14×10^{-14}	0.834	4822	6.69×10^{-13}	2.03×10^{-12}	3.80×10^{-12}	>1000	G2M	20
A2 + C_2H_2 → A3	4.10×10^{-18}	1.77	2395	2.65×10^{-13}	7.96×10^{-13}	1.60×10^{-12}	300−2000	exp./BAC-MP4	62
A2 + C_2H_2 → A3	2.63×10^{-11}	0	9832	2.32×10^{-13}	1.12×10^{-12}	2.47×10^{-12}	1000−1330	exp.	63
A2 + C_2H_2 → A3	6.64×10^{-17}	1.56	3800	5.11×10^{-13}	1.77×10^{-12}	3.76×10^{-12}	500−2500	AM1/RRKM	12
N2 + C_2H_2 → N3	2.12×10^{-18}	2.05	1930	1.18×10^{-12}	3.66×10^{-12}	7.67×10^{-12}	300−3000	G3[b]	this work
N2 + C_2H_2 → N3				4.76×10^{-13}	1.80×10^{-12}	4.33×10^{-12}	300−3000	G3	this work
A3 + C_2H_2 → A4	4.35×10^{-18}	2.0	4580	4.85×10^{-13}	2.26×10^{-12}	5.78×10^{-12}	300−3000	G3[b]	this work
A3 + C_2H_2 → A4				4.11×10^{-13}	2.33×10^{-12}	6.89×10^{-12}	300−3000	G3	this work
A3a + C_2H_2 → A4b	1.24×10^{-18}	1.98	5066	9.59×10^{-14}	4.77×10^{-13}	1.26×10^{-12}	300−3000	G3[b]	this work
A3a + C_2H_2 → A4b				6.78×10^{-14}	4.11×10^{-13}	1.25×10^{-12}	300−3000	G3	this work
A6 + C_2H_2 → A8	5.02×10^{-21}	2.55	3181	4.67×10^{-14}	2.19×10^{-13}	5.87×10^{-13}	300−3000	G3	this work
A11 + C_2H_2 → A12	2.23×10^{-20}	2.50	1283	3.76×10^{-13}	1.27×10^{-12}	2.90×10^{-12}	300−3000	G3	this work
Ring Closure (Radical Cyclization)									
A4b → A5	3.61×10^{9}	0.601	3635	4.07×10^{10}	9.27×10^{10}	1.47×10^{11}	300−3000	G3[b]	this work
A4b → A5				5.19×10^{10}	9.74×10^{10}	1.34×10^{11}	300−3000	G3	this work
A8 → A9	5.14×10^{12}	0.056	2127	2.71×10^{12}	3.90×10^{12}	4.70×10^{12}	300−3000	G3	this work
A12 → A13	9.95×10^{11}	0.045	5395	1.01×10^{11}	2.45×10^{11}	3.83×10^{11}	300−3000	G3	this work
N3 → N4	2.88×10^{11}	0.225	17 027	3.76×10^{8}	6.39×10^{9}	2.66×10^{10}	300−3000	G3	this work
cyclization of butylbenzene radical	4.60×10^{9}	0	11 496	1.82×10^{7}	1.15×10^{8}	2.90×10^{8}	100−1100	B3LYP/TST	68
Hydrogen Atom Loss									
A5 → N1 + H	7.16×10^{10}	0.756	15 144	9.09×10^{9}	1.45×10^{11}	6.00×10^{11}	300−3000	G3	this work
A9 → N1 + H	6.09×10^{10}	0.867	29 169	1.96×10^{7}	3.11×10^{9}	4.09×10^{10}	300−3000	G3	this work
A3 → A10 + H	7.18×10^{10}	1.02	38 674	6.66×10^{5}	5.19×10^{8}	1.53×10^{10}	300−3000	G3	this work
A3 → A10 + H	3.80×10^{11}	0.82	38 910	8.13×10^{5}	5.82×10^{8}	1.67×10^{10}	>1000	G2M	20
$C_6H_5CCH_2$ → A10 + H	1.23×10^{13}	0.55	42 580	6.97×10^{5}	8.05×10^{8}	2.87×10^{10}	>1000	G2M	20
N4 → AN + H	1.02×10^{11}	0.862	27 663	6.54×10^{7}	8.14×10^{9}	9.48×10^{10}	300−3000	G3	this work
Hydrogen Disproportionation									
A5 + H → N1 + H_2	3.51×10^{-15}	1.08	2011	2.34×10^{-12}	4.91×10^{-12}	7.92×10^{-12}	300−3000	G3	this work
A9 + H → N1 + H_2	3.40×10^{-16}	1.25	3405	3.56×10^{-13}	1.01×10^{-12}	1.91×10^{-12}	300−3000	G3	this work
A3 + H → A10 + H_2	2.74×10^{-13}	0.490	10 630	4.78×10^{-14}	3.11×10^{-13}	8.55×10^{-13}	300−3000	G3[b]	this work
N4 + H → AN + H_2	2.04×10^{-15}	0.984	9589	1.81×10^{-14}	1.22×10^{-13}	3.54×10^{-13}	300−3000	G3	this work
Acetylene Cycloaddition									
N1 + C_2H_2 → N5	5.18×10^{-22}	2.66	67 609	3.78×10^{-28}	5.70×10^{-23}	2.79×10^{-20}	300−3000	G3	this work
B1 + C_2H_2 → B2	2.81×10^{-23}	2.60	42 193	2.65×10^{-24}	6.60×10^{-21}	4.12×10^{-19}	300−3000	G3	this work
P + C_2H_2 → P1	7.18×10^{-23}	2.58	41 945	6.92×10^{-24}	1.64×10^{-20}	1.0×10^{-18}	300−3000	G3	this work
H_2 Loss									
N5 → AN + H_2	1.33×10^{10}	0.783	24 012	2.82×10^{7}	1.86×10^{9}	1.61×10^{10}	300−3000	G3	this work
B2 → P + H_2	4.73×10^{9}	0.797	17 176	2.95×10^{8}	6.53×10^{9}	3.28×10^{10}	300−3000	G3	this work
P1 → PYR + H_2	4.52×10^{10}	0.533	17 938	3.16×10^{8}	7.29×10^{9}	3.60×10^{10}	300−3000	G3	this work

[a] Units for the A factors and rate constants are s^{-1} and $cm^3\ s^{-1}$ molecule^{-1} for the unimolecular and bimolecular steps, respectively. [b] Computed by treating low-frequency modes as free rotors. Otherwise, all frequency modes were treated as harmonic oscillators during calculation of partition functions. [c] Recommended expressions obtained using combined experimental data and applying the unit-weighted least-squares analysis. [d] Rate expression obtained using the rate expression for the A2 + CH_4 → A1 + CH_3 step, $k(T) = 6.46 \times 10^{-27} T^{4.57} \exp(-5498/RT)$ $cm^3\ s^{-1}$ mol^{-1}, and the expression for the equilibrium constant, $K_{eq}(T) = (2.85 \pm 0.42) \times 10^{-2} T^{0.34} \pm 0.02 \exp(4438.2 \pm 16.1/T)$.[19]

for the C_6H_6 + H reaction. In other words, the higher rate of the C_6H_6 + H abstraction is attributed to its higher reaction path degeneracy. For the same reason, a similar large difference in rate constants is found for the C_6H_6 + OH and N1 + OH abstraction reactions, which also have similar barrier heights of 5.5 and 6.3 kcal/mol, respectively. Thus, the use of the common rate expressions, such as those proposed by Kiefer et al.[49] for C_6H_6 + H and by Madronich and Felder[51] for C_6H_6 + OH, is not a good assumption if applied to any H-abstraction process from aromatic hydrocarbons other than C_6H_6. The error in the rate coefficients in this case may exceed an order of magnitude even if the activation energy is expected to be similar to that for the model C_6H_6 + H/OH reactions. In this view, the use of the Reaction Class Transition State Theory/Linear Energy Relationship approach to predict rate constants for a group of similar reactions of related hydrocarbons suggested by Truong and co-workers is a better alternative.[61]

Because the A7 intermediate has one very low-frequency mode of 21 cm^{-1} corresponding to the internal rotation of the vinyl group, we expected a significant effect on the partition function of A7 and, therefore, on the rate constants for the A7 + H abstraction reaction if this mode is treated as a free rotor rather than a harmonic oscillator. However, as seen in Table 3, this is not the case; the rate constants calculated within the two models differ only slightly, indicating that anharmonicity associated with the rotational motion of the vinyl group in A7 does not affect the reaction rate significantly, apparently because of large moments of inertia for rotation around the C−C bond, 1.46×10^{-38} and 3.2×10^{-39} g cm^2 for the phenyl and vinyl fragments, respectively.

The available rate expressions for the H-abstractions by an OH radical are presented in Table 3, along with our fitted expressions for the C_6H_6 + OH and N1 + OH reactions. For C_6H_6 + OH, the agreement between our results and the G3/TST computed rate constants of Tokmakov and Lin[17] is found to be within a factor of 1.63 at typical combustion temperatures, although in our treatment, we considered all frequency modes in TS1b, including the low-frequency (100 cm^{-1}) OH-torsional mode, as harmonic oscillators, whereas Tokmakov and Lin[17] applied the hindered rotor treatment for this mode. Also, the agreement with the experimental data of Madronich and Felder,[51] Atkinson,[52] and Baulch et al.[53] is satisfactory; the largest deviation is a factor of 4.38. Significant disagreement (about 1 order of magnitude) is found only with the rate suggested in early experiments.[50] For the N1 + OH abstraction, the agreement of the calculated rate constants with the low-temperature experimental kinetic data of Atkinson[52] is worse, in the range of 1 order of magnitude. According to our G3/TST calculations, the C_6H_6 + OH abstraction reaction exhibits about 1 order of magnitude higher rate constants as compared to those for the abstraction by an H radical, C_6H_6 + H, at typical combustion temperatures (T < 1500 K), but at higher temperatures, their rates become similar. Such a behavior has an obvious explanation; at lower temperatures, the C_6H_6 + OH abstraction is faster because of a significantly lower barrier height, but as temperature increases, the C_6H_6 + H rate constant grows almost 3 times as fast as that for C_6H_6 + OH because of the higher barrier height. If the concentrations of H and OH radicals are comparable, then C_6H_6 + OH must be the dominant channel for H abstraction at combustion temperatures ($T \sim$ 1500 K), whereas at higher temperatures, one should expect a competition between the C_6H_6 + H and C_6H_6 + OH abstractions.

In calculations of rate constants for the C_6H_6 + CH_3 reaction, we applied a free internal rotor treatment for the lowest frequency mode (16 cm^{-1}) in TS1c, whereas the other two low-frequency C−H−C bending modes (85−90 cm^{-1}) were treated as harmonic oscillators. Although Tokmakov et al.[19] considered these two modes as hindered rotors, our results coincide with those by Tokmakov et al. within a factor of 2. On the other hand, because the rotation of the CH_3 group in TS1c is almost free, this mode should be treated as a rotor, not a harmonic oscillator, otherwise large errors occur in the rate constants (see Table 3). We were able to find only two sets of low-temperature experimental kinetic data for the C_6H_6 + CH_3 abstraction.[56,57] The agreement with these data is close for 1000 K; however, if we extrapolate the experimental rate expressions to high temperatures, the deviations are significant. New experimental measurements are suggested to verify our and Tokmakov et al.'s[19] high-temperature rate constants.

3.2. Acetylene Addition to the Radical Site. A. Ab Initio Calculations. The next step in the HACA PAH growth is acetylene addition (or consecutive additions) to the radical site. In our networks, we considered the addition of an acetylene molecule to phenyl and naphthyl radicals (C_6H_5 + C_2H_2 and N2 + C_2H_2), the addition of a second acetylene to the aromatic ring of the A6 and A11 radical intermediates (A6 + C_2H_2, A11 + C_2H_2), which represents Frenklach's variations of the HACA mechanism, and the addition of a second acetylene to the first one (A3 + C_2H_2, A3a + C_2H_2) taking part in Bittner−Howard's route of HACA synthesis.

All computed acetylene addition steps exhibit low barriers of 2−6 kcal/mol and are highly exothermic, by about 40 kcal/mol (see Table 1). The respective transition states TS2, TS3, TS7b, TS9, TS14, and $TS2^{AN}$ have tight, reactant-like structures (Figure 2). As seen in Table S1 of the Supporting Information, the acetylene addition transition states have several low-frequency modes (<100 cm^{-1}): 25, 64, and 93 cm^{-1} (TS2); 16, 44, 52, and 73 cm^{-1} (TS3); 19 and 52 cm^{-1} (TS7b); 45 and 76 cm^{-1} (TS9); 41, 68, and 89 cm^{-1} (TS14); and 33, 51, and 98 cm^{-1} ($TS2^{AN}$). The lowest mode corresponds to the internal rotation of the HCCH fragment around the forming C−C bond, whereas the other low frequencies are due to bending of the acetylene fragment.

The highest barrier in this reaction class is found for the C_2H_2 addition to the phenylvinyl radical (A3a) and the lowest barrier for the addition to the 2-ethynylphenyl radical (A11). Interestingly, the barrier for the C_2H_2 addition to the 1-naphthyl radical is considerably lower than that for the addition to the phenyl radical. The reaction enthalpies vary slightly, with the lowest exothermicity of 32.7 kcal/mol calculated for A3a + C_2H_2. The agreement between the barrier heights and reaction enthalpies computed by the B3LYP and G3 methods (see Table 1) is reasonably good;

as compared to G3, B3LYP overestimates the barriers by about 1−2 kcal/mol and underestimates the reaction exothermicity by 1−3 kcal/mol. Thus, B3LYP performs better in describing the reaction energetics of acetylene addition steps than for the hydrogen abstraction reactions discussed in the previous section.

Recent G2M calculations of Tokmakov and Lin[20] gave the barrier height for the $C_6H_5 + C_2H_2 \rightarrow C_6H_5CH{=}CH$ reaction as 3.5 kcal/mol, the same value as our G3 result. For the reaction enthalpy, the agreement is also close; their G2M value is only 1.2 kcal/mol lower (−40.4 kcal) than our prediction (−39.2 kcal/mol). Utilizing experimental heats of formation available for the phenyl radical and acetylene and isodesmic enthalpy of formation of phenylvinyl radical (A3a), the experimental estimation for the reaction enthalpy at 0 K is -39.6 ± 2.8 kcal/mol,[20] close to our value. Available experimental kinetic data[62−64] provide different values for the activation energy of acetylene addition to a phenyl radical. For example, the activation energy of 3.1 kcal/mol from the Arrhenius expression $2.2 \times 10^{11} \exp(-1560/T)$ cm^3 mol^{-1} s^{-1} ($T = 297-523$ K, $P = 20$ Torr) obtained by Yu et al.[62] in a low-temperature cavity ring-down experiment is in good agreement with our calculated barrier and with the results of Tokmakov and Lin.[20] The other two experimental reports[63,64] give significantly higher values for the barrier height, 9.8 kcal/mol from the very-low-pressure pyrolysis/mass spectroscopy study of Fahr et al.[63] and 8.0 kcal/mol from the shock tube/UV absorption study of Heckmann et al.[64] We tend to believe that, because the results of two accurate theoretical calculations (the present G3 study and the G2M study of Tokmakov and Lin[20]) are reliable, only the experimental data of Yu et al.[62] provide the most reasonable estimate for the barrier height of the $C_6H_5 + C_2H_2$ reaction, although their measurements were performed only at low temperatures and within a narrow temperature range.

3.2.B. Rate Constant Calculations. The calculation of rate constants corresponding to the acetylene addition steps requires taking into account the anharmonic effects due to low-frequency internal rotations of the C_2H_2 fragment in the corresponding transition states. Several transition states, TS2, TS3, TS7b, TS2^{AN}, and intermediate A4b, have very low-frequency modes (∼20 cm^{-1}), which can be treated either as free or hindered rotors. As seen in Table 3, the effect of the free-rotor treatment (instead of the use of a harmonic oscillator) is not as dramatic as in the case of the $C_6H_6 + CH_3$ reaction, which can be possibly attributed to significantly larger moments of inertia of the rotating C_2H_2 fragment. The free-rotor treatment increases the rate constants by a factor of 1.5−2 as compared to the harmonic oscillator model, and the effect increases with the temperature decrease. The maximal effect is found for the acetylene addition to the naphthyl radical (N2).

For the $C_6H_5 + C_2H_2$ reaction, our computed rate constants overestimate the recent G2M/RRKM results of Tokmakov and Lin[20] by a factor of 2.5−4. However, to better reproduce their experimental kinetic data, Tokmakov and Lin adjusted the G2M computed barrier height of 3.7 kcal/mol to a slightly higher value of 4.1 kcal/mol, whereas in our calculation, we used a lower value of 3.5 kcal/mol computed at the G3 level. The other sets of available experimental and theoretical data provide even lower values of rate constants in the temperature range of 1000−2000 K. For instance, 6−9 times lower values of rate constants were obtained in the experimental study of Yu et al.[62] combined with theoretical BAC-MP4/RRKM calculations and 5−7 times lower values were measured in the low-pressure pyrolysis/mass spectroscopy study of Fahr et al.[63] It is worth noting that the rate expression by Fahr et al.[63] is commonly used for the rate constants of acetylene addition reactions.

According to our calculations, acetylene addition to a phenyl radical has higher rates as compared to the other acetylene addition reactions. Acetylene addition to the A3 isomer of a phenylvinyl radical is significantly (by a factor of 4.5−5) faster than the addition to the A3a isomer. The acetylene addition to a naphthyl radical (N2) has rate constants 1.5−2 times lower than those for the addition to a phenyl radical. The A6 + C_2H_2 reaction exhibits the largest difference for the rate constants (25−36 times lower values) as compared to the $C_6H_5 + C_2H_2$ reaction. Thus, the individual rates for the acetylene addition steps may significantly vary depending on the structure of the reacting radical, and the use of a common rate expression for all acetylene additions to PAH intermediates may result in significant errors and dramatically affect the kinetic modeling results.

Two acetylene addition reactions considered here, A3a + C_2H_2 (to the vinyl chain of a phenylvinyl radical) and A11 + C_2H_2 (to the aromatic ring of a 2-ethynylphenyl radical) are of a special interest in the HACA synthesis, as the former belongs to Bittner−Howard's route (the second acetylene molecule adds to the first one) and the latter is a part of Frenklach's route (the second acetylene adds to the aromatic ring). Acetylene addition to the A3 isomer of a phenylvinyl radical is not relevant because the subsequent rearrangements to the A4b intermediate are energetically and kinetically unfavorable. According to our calculations, at combustion temperatures, the A11 + C_2H_2 addition (Frenklach's route) exhibits 2.3−3.9 times higher rates as compared to the A3a + C_2H_2 addition (Bittner−Howard route).

3.3. Ring Closure Steps. Cyclization steps in the naphthalene formation network are the following: A4b → A5, A8 → A9, and A12 → A13 (see Figure 1). The N3 → N4 ring closure in the acenaphthalene network leads to the formation of a five-membered ring—a substructure of cyclopentafused PAH. All the cyclization steps can be defined as intramolecular additions either to the aromatic C−C bond (A4b → A5 and N3 → N4) or to the double (A8 → A9) or triple (A12 → A13) bonds. Additionally, the A4b → A5 and N3 → N4 steps represent ring closure between a hydrocarbon radical chain and the aromatic ring, whereas the A8 → A9 and A12 → A13 cyclizations involve reactions between two hydrocarbon chains (vinyl and ethynyl) attached to the aromatic ring.

The A4b → A5, A8 → A9, and A12 → A13 cyclization steps exhibit low barriers (1.8−5.4 kcal/mol) and are highly exothermic. The five-membered ring formation in the acenaphthalene core via N3 → N4 is found to have a much higher barrier of 16.6 kcal/mol and a lower exothermicity

as compared to those of the other cyclization steps. This result can be explained if we analyze the structure of the corresponding transition state $TS3^{AN}$ (see Figure 2); the naphthyl fragment in this transition state is nonplanar and differs significantly from that in the reactant, N3 radical. Thus, the ring closure N3 → N4 requires a significant deformation of the reactant molecule in the transition state, apparently because of the steric repulsion. The lowest barrier of 1.8 kcal/mol is found for the A8 → A9 step, which is an example of intramolecular addition to the vinyl double bond. The addition to the ethynyl triple bond (A12 → A13) has a 3 times higher barrier height, 5.4 kcal/mol. The transition state TS10, which corresponds to the A8 → A9 step, is found to have the lowest imaginary frequency of $90i$ cm^{-1}. The analysis of its structure, vibrational frequencies, and the results of IRC calculations show that the ring closure A8 → A9 occurs simultaneously with the rotation of the vinyl fragment around the C−C bond. In accord with the high exothermicity of the ring closure reactions, all respective transition states exhibit an early, reactant-like character.

The agreement between G3- and B3LYP-computed barrier heights and reaction exothermicities for the A4b → A5, A8 → A9, and A12 → A13 ring closure steps is found to be within 0.5−1.0 and within 3 kcal/mol for barriers and reaction enthalpies, respectively. Therefore, B3LYP can perform well in predicting the energetics for these kind of reactions. This is not surprising as a similarly impressive agreement between the high-level CBS−RAD method and B3LYP was also demonstrated[65] for the ring opening of the cyclopropylcarbinyl radical. Up to now, the mechanism of radical cyclization reactions was scarcely studied by high-level ab initio methods. We were able to find only a few DFT studies of analogous reaction steps relevant to the PAH synthesis. Bauschlicher and Ricca[21] computed barrier heights and reaction enthalpies of the A12 → A13 and A4b → A5 cyclization steps at the B3LYP/4-31G level. For A12 → A13, their barrier height of 4.5 kcal/mol and reaction enthalpy of −56.5 kcal/mol are similar to our B3LYP predictions (4.8 and −53.8 kcal/mol, respectively) obtained with the significantly larger basis set. For the A4b → A5 ring closure, the agreement with our B3LYP calculations is notably worse; their computed barrier and reaction enthalpy are 7.3 and −23.6 kcal/mol, respectively, at the B3LYP/4-31G level versus our values of 4.6 and −29.3 kcal/mol, respectively, at the B3LYP/6-311+G(3df,2p) level.

B3LYP/6-311G** calculations were also applied earlier to investigate the mechanism of cyclization reactions for the alkyl chain radicals bonded to various PAHs including benzene, naphthalene, anthracene, and so forth, containing 1−4 aromatic rings.[66−68] The calculated barriers were found to be significantly higher as compared to those of our predictions for the cyclization involving vinyl-type radical side chains and varied from 8.0 to 12.0 kcal/mol depending on the PAH. For instance, for the $C_6H_5-C_4H_8$ (1-phenylbutyl) radical, the barrier for the ring closure was calculated to be 11.8 kcal/mol,[68] whereas our predictions for the cyclization barriers of the A4b radical are 3.6 and 4.6 kcal/mol at the G3 and B3LYP levels, respectively. Such a difference in the calculated barrier heights may originate from the different reactivities of the C_4H_8 (alkyl, single C−C bond) and C_4H_4 (vinyl-type, double C=C bond) radical chains involved in cyclization.

According to the recent G2M study of Tokmakov and Lin,[20] the formation of a four-membered ring of the benzenecyclobutadiene core in the radical cyclization of phenylvinyl radical (A3) and 1-vinyl-2-phenyl radical (A6) was found to be considerably less energetically favorable than cyclizations leading to five- or six-membered rings in naphthalene or acenaphthalene. Indeed, the ring closure of the phenylvinyl radical giving the bicyclo[4.2.0]octa-2,4,7-trien-1-yl radical intermediate requires overcoming a barrier of 33.4 kcal/mol, and a similar barrier of 32.1 kcal/mol was found for the cyclization of the 2-vinylphenyl radical producing bicyclo[4.2.0]octa-1,3,5-trien-7-yl. Significantly lower barriers of 10.1 and 12.5 kcal/mol at the CBS−RAD and G2M(RCC) levels, respectively, were obtained by Smith et al.[65] for the formation of a three-membered ring in the cyclopropylcarbinyl radical. However, their values are also much higher than the barriers for the formation of the second aromatic ring in naphthalene calculated here.

As seen in Table 3, rate constants for the ring closure steps at combustion-relevant temperatures significantly differ from each other and increase in the row: k(N3 → N4) < k(A4b → A5) < k(A12 → A13) < k(A8 → A9). The highest rate is found for the A8 → A9 reaction, in line with the lowest barrier height for this step. Also, the lowest rate for the N3 → N4 ring closure can be attributed to the highest reaction barrier of 16.6 kcal/mol. However, as the temperature increases, the differences between various cyclization rate constants significantly decrease. Available kinetic data for the radical cyclization of the primary butylbenzene radical[68] are compared with our results in Table 3. It can be seen that cyclization involving a single bond of the alkyl radical chain attached to the aromatic ring exhibits significantly lower reaction rates as compared to cyclizations involving double (A4b → A5) or triple (A12 → A13) bonds. This confirms the advantage of the HACA scheme of PAH synthesis with respect to the other mechanisms involving PAH with side alkyl chains.

3.4. Hydrogen Loss/Disproportionation. The reactions of radical cyclization lead to the formation of an additional ring in the forming PAH core. Depending on the hydrocarbon side chains involved in the ring closure, the resulting PAH molecule may contain "extra" hydrogen atoms, like in A5, A9, and N4 intermediates. Elimination of these hydrogen atoms from the radical intermediates together with reactions of radical recombination represent the final steps in the HACA synthesis of larger, stable PAH species. Another important role of hydrogen elimination is to form singlet PAH intermediates with side chains (e.g., phenylacetylene A10), which are involved in further PAH synthesis or represent abundant byproducts in flame combustion. It is commonly assumed that H elimination from radical intermediates at combustion conditions can be realized by the direct hydrogen loss mechanism, which normally has a high barrier. According to our G3 calculations and results of other ab initio studies of similar reactions,[20] the barriers for the H loss from radical intermediates are in the range of several

tens of kilocalories per molecule (see Table 1) and these reactions are highly endothermic. In our previous study[22] of the HACA phenanthrene synthesis, we proposed an alternative hydrogen disproportionation mechanism, which involves free H radicals in the elimination of extra hydrogen atoms (the other abundant small radicals, like OH, CH_3, etc., may also play a similar role). We showed that the disproportionation mechanism is energetically more favorable than the H-atom loss mechanism; the computed barriers for the former are much lower than those for the latter.

Accurate calculations of PESs for hydrogen disproportionation reactions represent a challenging problem because, during this process, the wave function character changes from open-shell to closed-shell singlet. By applying the UB3LYP method, we were often unable to reach convergence during geometry optimization of the H-disproportionation open-shell singlet transition states. To solve this problem, in our previous study, we employed the multireference CASSCF method with the 6-31G* basis set for calculation of reaction barriers; however, because of the large size of the molecules, the calculations were limited to a small (4,6) active space. To make more reliable predictions of the reaction barriers, more sophisticated methods must be applied. In the present study, we utilized the IRCMax{Energy[G3(MP2,CC)]}//IRC-{Geom[UMP2/6-31G*]} method instead of B3LYP or HF. Using UMP2 for geometry optimization, we were able to locate open-shell singlet transition states TS6a, TS11a, TS12a, and TS4a^{AN}. Then, IRC calculations were performed to confirm that the optimized transition state structures actually correspond to the H-disproportionation reaction path. The single-point energies of the transition states and several structures along the minimal energy reaction path obtained by IRC calculations were refined at the G3 level, with the UMP2 frequencies, geometries, and ZPE corrections. Thus, we expect that the accuracy of barrier heights calculated using the IRCMax approach should be close to that anticipated from G3 calculations.

As seen in Table 1, for the A5 → N1, A9 → N1, A3 → A10, and N4 → AN reaction steps, the calculated barriers for H disproportionation are respectively 12.1, 22.8, 24.6, and 15.7 kcal/mol lower as compared to those for H loss. For the reaction enthalpies, the difference is even more dramatic; the disproportionation mechanism is strongly exothermic, by 75−125 kcal/mol, whereas the H loss exhibits an endothermicity of several tens of kilocalories per molecule, except for the A5 → N1 + H reaction, which is only 2.5 kcal/mol endothermic. The H-disproportionation transition states TS6a, TS11a, TS12a, and TS4a^{AN} are more reactant-like, whereas the direct H-loss transition states TS6, TS11, TS12, and TS4^{AN} exhibit more product-like structures. For TS12a, we found a very low-frequency mode of 12 cm^{-1} corresponding to high-amplitude torsional motion of the C_2H_3 fragment around the $C_{Phenyl}-C_{Vinyl}$ bond. During rate constant calculation, this low frequency was treated as a free internal rotor.

Several theoretical predictions of the reaction barriers and enthalpies for the direct H-atom loss reactions can be found in the literature.[20−22,69] Tokmakov and Lin[20] applied G2M theory to compute the PES for the $C_6H_5 + C_2H_2$ reaction including two H-loss steps, from 1-phenylvinyl ($C_6H_5C=CH_2$) and phenylvinyl (A3) radicals. Both reactions have the same product, phenylacetylene (A10). For the former, their computed barrier and reaction enthalpy are 41 and 38.6 kcal/mol, respectively. The H loss from the A3 radical exhibits a barrier of 38 kcal/mol and a reaction enthalpy of 31.5 kcal/mol at the G2M level, which are slightly higher than our G3 values of 36.6 and 30.1 kcal/mol, respectively. The PES for the hydrogen loss from the allyl (C_3H_5) radical to form of a singlet allene was studied at the CCSD(T)/cc-pVTZ//MP4/6-31G* level,[69] and the reaction barrier and enthalpy were evaluated as 63.3 and 55.4 kcal/mol, respectively. The H loss from a cyclic intermediate, the cyclopropyl radical, to form cyclopropene was found to have ∼10 kcal/mol lower values for the barrier (52.1 kcal/mol) and reaction enthalpy (48.8 kcal/mol). These energies are significantly higher than the barrier and reaction enthalpy for the H loss from A3, indicating that the direct H loss is more favorable energetically from the cyclic PAH intermediates than from chain hydrocarbons.

Earlier,[70] we studied the $C_6H_5 + H$ disproportionation reaction at the G2M(cc,MP2) level and found the barriers of 7.6, 10.9, and 17.1 kcal/mol corresponding to the formation of *o*-C_6H_4, *m*-C_6H_4, and *p*-C_6H_4, respectively, whereas the computed heats of reaction were −29.1, −14.8, and −1.9 kcal/mol, respectively. Thus, the barriers for the disproportionation steps considered here are similar to that for $C_6H_5 + H \rightarrow o\text{-}C_6H_4 + H_2$, but their exothermicities are much higher because the products formed are more stable than benzyne. On the other hand, H elimination from C_6H_5 requires much higher barriers, especially to produce the *m*- and *p*-C_6H_4 isomers. Rate constant calculations[70] demonstrated that the $C_6H_5 + H \rightarrow o\text{-}C_6H_4 + H_2$ disproportionation channel can compete with the $C_6H_5 + H \rightarrow C_6H_6$ recombination only at high temperatures ($T > 2000$ K).

In our previous study of the HACA phenathrene synthesis, we applied lower-level B3LYP/6-31G* and CASSCF(4,6)/6-31G*//UHF/6-31G* calculations and considered both direct H loss and H disproportionation from various PAH radical intermediates. For the H-loss reactions similar to A5 → N1 + H, we obtained barriers of 16.6−19.0 kcal/mol and reaction enthalpies were in the range of 7.5−10.9 kcal/mol. For H disproportionation, barriers and reaction exothermicities were 0.9−5.8 and 92.5−95.9 kcal/mol, respectively. For the reaction steps similar to A9 → N1 + H, the barriers were 27.5−32.3 and 0.7−1.5 kcal/mol for the H loss and H disproportionation, respectively, and reaction enthalpies varied within 24.2−29.8 and −73.6 to −79.2 kcal/mol for the H-loss and disproportionation mechanisms, respectively. The reactions leading to acetylenic intermediates, like A3 → A10 + H, were shown to have barriers within 40.6−40.2 (H loss) and 4.7−9.5 kcal/mol (H disproportionation) and heats of reaction were 35.8−36.0 (H loss) and −67.4 to −67.7 kcal/mol (H disproportionation). These data demonstrate a close agreement between our earlier results for the H-elimination reactions from PAH radical intermediates (both for the H-loss and H-disproportionation mechanisms) obtained using lower-level ab initio methods and the present, supposedly more accurate, G3 values.

The calculated rate constants for the H-loss and H-disproportionation steps involved in the naphthalene and acenaphthalene formation networks are compared in Table 3. For A3 → A10 + H, the agreement of our G3/RRKM calculated rate constants with those reported by Tokmakov and Lin[20] is very close. Rate constants for the H-loss steps increase systematically with decreasing barrier heights; the lowest rate is found for the A3 → A10 + H reaction with the barrier of 36.6 kcal/mol, and the highest rate is calculated for A5 → N1 + H with the lowest barrier of 14.8 kcal/mol. As the hydrogen disproportionation steps have much lower barriers, their rate constants are much higher than those for the H-loss channels. We can conclude this from the comparison of the first-order rate constants for the H-loss steps with the second-order rate constants for the H-disproportionation steps converted to the $cm^3\ mol^{-1}\ s^{-1}$ units (see Table 2). For instance, at 1500 K, the rate constants are 1.4×10^{11} (3.0×10^{12}), 3.0×10^9 (6.2×10^{11}), 4.9×10^8 (2.0×10^{11}), and $7.9 \times 10^9\ s^{-1}$ ($7.6 \times 10^{10}\ cm^3\ mol^{-1}\ s^{-1}$) for the A5 → N1, A9 → N1, A3 → A10, and N4 → AN steps, respectively, where the H-disproportionation rate constants are given in parentheses. Another issue concerns equilibrium constants for the H-loss steps. As seen in Table 2, the rates for the backward reactions (hydrogen atom addition) are significantly faster as compared to those for the forward reactions, which are responsible for the H-atom removal from the PAH intermediate. The computed rate constants for the forward (reverse) reactions at 1500 K are 1.4×10^{11} (9.9×10^{11}), 3.0×10^9 (1.1×10^{13}), 4.9×10^8 (1.3×10^{13}), and $7.9 \times 10^9\ s^{-1}$ ($4.3 \times 10^{12}\ cm^3\ mol^{-1}\ s^{-1}$) for A5 → N1, A9 → N1, A3 → A10, and N4 → AN, respectively. Thus, the equilibrium of H-loss reactions is considerably shifted to the reactant species suppressing the production of singlet PAH molecules unless the H radicals are consumed in some other reactions. On the contrary, equilibrium constants for hydrogen disproportionation reactions are high (see Table 2), and therefore, the H-disproportionation steps can be considered as irreversible. However, the formation of singlet PAH species by the H-disproportionation mechanism can compete with their consumption in the H-addition reactions (reverse reactions for the H-loss steps), leading back to the reactant species. Indeed, if we compare the rate constants of the forward reactions for the H-disproportionation steps, A5 + H → N1 + H_2, A9 + H → N1 + H_2, A3 + H → A10 + H_2, and N4 + H → AN + H_2, with those for the H-atom additions, N1 + H → A5, N1 + H → A9, A10 + H → A3, and AN + H → N4, we find that the latter usually have 1 or 2 orders of magnitude higher rates (except for the A5 → N1 channel) than those of the former.

3.5. Acetylene Cycloaddition (Diels−Alder) Mechanism. Another possible mechanism of PAH formation in combustion flames, which does not involve radical species in any elementary step, is the so-called benzogenic Diels−Alder mechanism,[2] recently proposed to be the dominant route of PAH growth in methane combustion.[31] Together with the conventional HACA synthesis, the Diels−Alder mechanism was postulated as an important process in PAH growth.[31] To prove that the Diels−Alder mechanism is a viable alternative to HACA, accurate calculations of the reaction energetics and rate constants are required. Here, we calculated PESs and reaction rate constants for three Diels−Alder-type acetylene cycloadditions leading to the formation of acenaphthalene (AN), phenanthrene (P), and pyrene (PYR) starting from naphthalene (N1), biphenyl (B1), and phenanthrene (P), respectively (Figure 1). Previously, we studied the B1 → B2 → P reaction sequence at the B3LYP/6-31G* level,[22] and now, we have refined those results at the more accurate G3 level.

The acetylene cycloaddition pathways involve two consecutive elementary steps: [2+4] or [2+3] cycloaddition leading to a Diels−Alder adduct (N5, B2, and P1 intermediates) followed by elimination of H_2. The first step has a high barrier and is endothermic, but the second one is strongly exothermic and exhibits at least 2 times lower barriers. The [2+3] cycloaddition of an acetylene molecule to naphthalene shows a more than 20 kcal/mol higher barrier and a ∼40 kcal/mol higher endothermicity than the [2+4] cycloadditions (B1 + C_2H_2 and P + C_2H_2). The subsequent H_2 elimination from N5 has a 7−8 kcal/mol higher barrier but a considerably higher exothermicity than those for H_2 eliminations from B2 and P1. The trends in the computed rate constants for both acetylene cycloaddition and H_2-loss reactions are parallel to the respective barrier heights. For instance, the [2+3] cycloaddition reaction of acetylene to naphthalene is found to have a lower rate as compared to those for the reactions of C_2H_2 with biphenyl and phenanthrene. The same is true for the subsequent H_2 eliminations; the N5 → AN + H_2 reaction is slower than B2 → P + H_2 and P1 → PYR + H_2. Thus, the [2+3] cycloaddition to naphthalene followed by H_2 elimination is less energetically and kinetically favorable than the [2+4] cycloadditions and H_2 eliminations involving biphenyl and phenanthrene.

We found considerable discrepancies in B3LYP and G3 computed barriers and reaction enthalpies (especially for the latter) for the Diels−Alder steps. B3LYP overestimates barrier heights and reaction endothermicities for acetylene cycloaddition reactions by about 6 and 10 kcal/mol, respectively. For the H_2-elimination steps, the agreement in computed barriers is satisfactory (within 1−2 kcal/mol), but for reaction exothermicities, the B3LYP values overestimate G3 results by 6−8 kcal/mol. Surprisingly few theoretical studies have been carried out on Diels−Alder-type reactions relevant to the formation of PAH or other hydrocarbons abundant in combustion flames. A slightly modified version of the G2M method (G2MS)[71] has been applied by Froese at al. to calculate PESs for the analogous [2+4] cycloaddition of acetylene to butadiene and cyclopentadiene.[72] For these reactions, they found relatively high but almost 2 times lower barriers, 25.8 and 22.0 kcal/mol, respectively, as compared to those of the acetylene cycloaddition steps considered here. For the reaction enthalpies, the difference is even more dramatic; the reactions of acetylene with butadiene and cyclopentadiene are strongly exothermic (by −52.2 and −26.5 kcal/mol, respectively), in contrast to endothermic N1 + C_2H_2 → N5, B1 + C_2H_2 → B2, and P + C_2H_2 → P1 reactions. This can be explained by the higher stability of the reaction products (1,4-cyclohexadiene in the case of the

C_2H_2 + butadiene reaction) as compared to the lower stability of distorted structures of the N5, B2, and P1 Diels−Alder adducts with respect to the aromatic naphthalene, biphenyl, and phenanthrene molecules. Nevertheless, transition states $TS5^{AN}$, $TS1^{P}$, and $TS1^{PYR}$ have structures similar to those for the C_2H_2 + butadiene/cyclopentadiene reactions.

Owing to much higher barriers, all computed Diels−Alder acetylene cycloaddition steps, N1 + C_2H_2 → N5, B1 + C_2H_2 → B2, and P + C_2H_2 →P1, have rate constants several orders of magnitude (12−16, 8−13, and 7−9 orders of magnitude at 1000, 1500, and 2000 K, respectively) lower than the respective values for C_2H_2 addition to radical intermediates A2, A3, N2, A6, and A11. The difference is still large even at higher combustion temperatures of 2500−3000 K. For example, the rate constants for the N2 + C_2H_2 → N3 acetylene addition and the N1 + C_2H_2 → N5 Diels−Alder [2+3] cycloaddition reactions are respectively 1.4×10^{-11} and 1.9×10^{-17} cm^3 s^{-1} $molecule^{-1}$ at 3000 K. This strongly indicates that the Diels−Alder PAH synthesis cannot compete with the conventional HACA mechanism not only at low but also at high combustion temperatures.

4. Conclusions

Ab initio G3-type calculations of PESs and RRKM and TST calculations of reaction rate constants for the HACA mechanism of naphthalene and acenaphthalene synthesis and Diels−Alder reaction pathways leading to acenaphthalene, phenanthrene, and pyrene have been performed. The calculations allowed us, for the first time, to consider the HACA network as a whole, using the most reliable potential energy surfaces, which are expected to be accurate within 1−2 kcal/mol. The barrier heights, reaction energies, and molecular parameters of the reactants, products, intermediates, and transition states have been generated for all types of reactions involved in the HACA mechanism, including H abstraction from various aromatic intermediates, acetylene addition to radical sites, ring closures leading to the formation of additional aromatic rings, elimination of hydrogen atoms, and H disproportionation. The calculated energetic parameters and rate constants are compared with available literature data, both experimentally and theoretically obtained earlier using less accurate computational methods. A good agreement with experimental data has been found wherever the experimental data are available, and in general, the present G3 results are demonstrated to be more accurate than previous theoretical values calculated either by density functional methods or by G2 theory and its modifications.

The results show that the Diels−Alder mechanism cannot compete with the HACA pathways even at high combustion temperatures, because of high barriers and consequently low reaction rate constants. Alternatively, the reactions involved in various HACA sequences are demonstrated to have relatively low barriers and high rate constants under combustion conditions. A comparison of the significance of different HACA mechanisms (e.g., Frenklach's, alternative Frenklach's, and Bittner and Howard's routes) in PAH growth can be made in the future using PESs and molecular parameters obtained in the present work. To achieve this ultimate goal, pressure-dependent rate constants need to be calculated for each reaction step using RRKM theory, and then, kinetic modeling can be performed to estimate relative probabilities of different routes within the PAH formation networks. At real combustion conditions, many other important reaction steps, such as oxidation, radical recombination, and so forth, must be taken into account to predict the system evolution and product yields.

Our results also demonstrate that the use of common rate expressions based on kinetic data for the first aromatic ring (for example, for the C_6H_6 + H and C_6H_6 + OH reactions or acetylene addition to C_6H_5) in kinetic modeling of flame combustion is not a good approximation if applied to any H-abstraction or acetylene addition reactions involving aromatic hydrocarbons other than C_6H_6. The error in the rate coefficients, in this case, may exceed 1 order of magnitude even if the activation energy is expected to be similar to that for the model C_6H_6 + H/OH or C_6H_5 + C_2H_2 reactions. The individual reaction rates vary significantly depending on the structure of the reacting aromatic molecule or radical, and the use of common rate expressions may result in significant errors and dramatically affect the kinetic modeling results. The effect of the free-rotor treatment replacing the harmonic oscillator is significant only in the cases when the moments of inertia of rotating fragments are small, as for the transition state of the C_6H_6 + CH_3 reaction.

Acknowledgment. This work is funded by the Chemical Sciences, Geosciences and Biosciences Division, Office of Basic Energy Sciences, Office of Sciences of U.S. Department of Energy (Grant No. DE-FG02-04ER15570). We also thank Academia Sinica, National Science Council of Taiwan, R.O.C., for partial financial support.

Supporting Information Available: Vibrational frequencies, ZPEs, moments of inertia, rotational constants, and optimized Cartesian coordinates of all species involved in the studied PAH formation networks (Table S1); fitted rate expressions in the modified Arrhenius form $k = AT^n \exp(-E/RT)$ for the forward and reverse rate constants for all studied reactions (Table S2). This material is available free of charge via the Internet at http://pubs.acs.org.

References

(1) Grimmer, G. *Environmental Carcinogens: Polycyclic Aromatic Hydrocarbons: Chemistry, Occurrence, Biochemistry, Carcinogenity*; CRC Press: Boca Raton, FL, 1983.

(2) Ramdahl, T.; Bjorseth, J. *Handbook of Polycyclic Aromatic Hydrocarbons*, 2nd ed.; Marcel Dekker: New York, 1985; p 1.

(3) Perera, F. P. *Science* **1997**, *278*, 1068.

(4) Venkataraman, C.; Friedlander, S. K. *Environ. Sci. Technol.* **1994**, *28*, 563.

(5) Allen, J. O.; Dookeran, K. M.; Smith, K. A.; Sarofim, A. F.; Taghizadeh, K.; Lafleur, A. L. *Environ. Sci. Technol.* **1996**, *30*, 1023.

(6) Richter, H.; Howard, J. B. *Prog. Energy Combust. Sci.* **2000**, *26*, 565.

(7) Frenklach, M. *Phys. Chem. Chem. Phys.* **2002**, *4*, 2028.

(8) Cook, D. J.; Schlemmer, S.; Balucani, N.; Wagner, D. R.; Steiner, B.; Saykally, R. J. *Nature* **1996**, *380*, 227.

(9) Snow, T. P.; Le Page, V.; Keheyan, Y.; Bierbaum, V. M. *Nature* **1998**, *391*, 259.

(10) Frenklach, M.; Wang, H. *Proc. Combust. Inst.* **1991**, *23*, 1559.

(11) Frenklach, M.; Clary, D. W.; Gardiner, W. C.; Stein, S. E. *Proc. Int. Symp. Combust.* **1984**, *20*, 887.

(12) Wang, H.; Frenklach, M. *J. Phys. Chem.* **1994**, *98*, 11465.

(13) Appel, J.; Bockhorn, H.; Frenklach, M. *Combust. Flame* **2000**, *121*, 122.

(14) Bittner, J. D.; Howard, J. B. *Proc. Int. Symp. Combust.* **1981**, *18*, 1105.

(15) (a) Frenklach, M.; Moriarty, N. W.; Brown, N. J. *Proc. Combust. Inst.* **1998**, *27*, 1655. (b) Moriarty, N. W.; Brown, N. J.; Frenklach, M. *J. Phys. Chem. A* **1999**, *103*, 7127.

(16) Mebel, A. M.; Lin, M. C.; Yu, T.; Morokuma, K. *J. Phys. Chem. A* **1997**, *101*, 3189.

(17) Tokmakov, I. V.; Lin, M. C. *J. Phys. Chem. A* **2002**, *106*, 11309.

(18) Chen, C.-C.; Bozzelli, J. W. *J. Phys. Chem. A* **2004**, *108*, 4632.

(19) Tokmakov, I. V.; Park, J.; Gheyas, S.; Lin, M. C. *J. Phys. Chem. A* **1999**, *103*, 3636.

(20) Tokmakov, I. V.; Lin, M. C. *J. Am. Chem. Soc.* **2003**, *125*, 11397.

(21) Bauschlicher, C. W.; Ricca, A. *Chem. Phys. Lett.* **2000**, *326*, 283.

(22) Kislov, V. V.; Mebel, A. M.; Lin, S. H. *J. Phys. Chem. A* **2002**, *106*, 6171.

(23) Miller, J. A.; Melius, C. F. *Combust. Flame* **1992**, *91*, 21.

(24) Melius, C. F.; Colvin, M. E.; Marinov, N. M.; Pitz, W. J.; Senkan, S. M. *Proc. Int. Symp. Combust.* **1996**, *26*, 685.

(25) Marinov, N. M.; Pitz, W. J.; Westbrook, C. K.; Vincitore, A. M.; Castaldi, M. J.; Senkan, S. M.; Melius, C. F. *Combust. Flame* **1998**, *114*, 192.

(26) Madden, L. K.; Mebel, A. M.; Lin, M. C.; Melius, C. F. *J. Phys. Org. Chem.* **1996**, *9*, 801.

(27) Miller, J. A.; Klippenstein, S. J. *J. Phys. Chem. A* **2003**, *107*, 7783.

(28) Howe, P.-T.; Fahr, A. *J. Phys. Chem. A* **2003**, *107*, 9603.

(29) Shafir, E. V.; Slagle, I. R.; Knyazev, V. D. *J. Phys. Chem. A* **2003**, *107*, 8893.

(30) Richter, H.; Howard, J. B. *Phys. Chem. Chem. Phys.* **2002**, *4*, 2038.

(31) Siegmann, K.; Sattler, S. *J. Chem. Phys.* **2000**, *112*, 698.

(32) (a) Becke, A. D. *J. Chem. Phys.* **1992**, *96*, 2155. (b) Becke, A. D. *J. Chem. Phys.* **1992**, *97*, 9173. (c) Becke, A. D. *J. Chem. Phys.* **1993**, *98*, 5648. (d) Lee, C.; Yang, W.; Parr, R. G. *Phys. Rev. B* **1988**, *B37*, 785. (e) Kang, J. K.; Musgrave, C. B. *J. Chem. Phys.* **2001**, *115*, 11040.

(33) Curtiss, L. A.; Raghavachari, K.; Redfern, P. C.; Rassolov, V.; Pople, J. A. *J. Chem. Phys.* **1998**, *109*, 7764.

(34) (a) Baboul, A. G.; Curtiss, L. A.; Redfern, P. C.; Raghavachari, K. *J. Chem. Phys.* **1999**, *110*, 7650. (b) Curtiss, L. A.; Raghavachari, K.; Redfern, P. C.; Baboul, A. G.; Pople, J. A. *Chem. Phys. Lett.* **1999**, *314*, 101.

(35) The G3large and G3MP2large basis sets can be downloaded from http://chemistry/anl.gov/compmat/g3theory.htm.

(36) (a) Malick, D. K.; Petersson, G. A.; Montgomery, J. A., Jr. *J. Chem. Phys.* **1998**, *108*, 5704. (b) Chuang, Y. Y.; Corchado, J. C.; Truhlar, D. G. *J. Phys. Chem. A* **1999**, *103*, 1140.

(37) Hehre, W. J.; Radom, L.; Schleyer, P. V. R.; Pople, J. A. *Ab Initio Molecular Orbital Theory*; Wiley: New York, 1986.

(38) (a) Gonzalez, C.; Schlegel, H. B. *J. Chem. Phys*. **1989**, *90*, 2154. (b) Gonzalez, C.; Schlegel, H. B. *J. Phys. Chem*. **1990**, *94*, 5523.

(39) Frisch, M. J.; Trucks, G. W.; Schlegel, H. B.; Scuseria, G. E.; Robb, M. A.; Cheeseman, J. R.; Zakrzewski, V. G.; Montgomery, J. A.; Stratmann, R. E.; Burant, J. C.; Dapprich, S.; Millam, J. M.; Daniels, R. E.; Kudin, K. N.; Strain, M. C.; Farkas, O.; Tomasi, J.; Barone, V.; Cossi, M.; Cammi, R.; Mennucci, B.; Pomelli, C.; Adamo, C.; Clifford, S.; Ochterski, J.; Petersson, G. A.; Ayala, P. Y.; Cui, Q.; Morokuma, K.; Salvador, P.; Dannenberg, J. J.; Malick, D. K.; Rabuck, A. D.; Raghavachari, K.; Foresman, J. B.; Cioslowski, J.; Ortiz, J. V.; Baboul, A. G.; Stefanov, B. B.; Liu, G.; Liashenko, A.; Piskorz, P.; Komaromi, I.; Gomperts, R.; Martin, R. L.; Fox, D. J.; Keith, T.; Al-Laham, M. A.; Peng, C. Y.; Nanayakkara, A.; Challacombe, M.; Gill, P. M. W.; Johnson, B.; Chen, W.; Wong, M. W.; Andres, J. L.; Gonzalez, C. M.; Head-Gordon, M.; Replogle, E. S.; Pople, J. A. *Gaussian 98*, revision A.11; Gaussian, Inc.: Pittsburgh, PA, 2001.

(40) Werner, H.-J.; Knowles, P. J. *MOLPRO*, version 2002.1. Amos, R. D., Bernhardsson, A., Berning, A., Celani, P., Cooper, D. L., Deegan, M. J. O., Dobbyn, A. J., Eckert, F., Hampel, C., Hetzer, G., Knowles, P. J., Korona, T., Lindh, R., Lloyd, A. W., McNicholas, S. J., Manby, F. R., Meyer, W., Mura, M. E., Nicklass, A., Palmieri, P., Pitzer, R., Rauhut, G., Schutz, M., Schumann, U., Stoll, H., Stone, A. J., Tarroni, R., Thorsteinsson, T., Werner, H.-J., Eds.

(41) Steinfield, J.; Francisco, J.; Hase, W. *Chemical Kinetics and Dynamics*; Prentice Hall: Englewood Cliffs, NJ, 1989.

(42) Eyring, H.; Lin, S. H.; Lin, S. M. *Basic Chemical Kinetics*; Wiley: NewYork, 1980.

(43) Robinson, P. J.; Holbrook, K. A. *Unimolecular Reactions*; Wiley: NewYork, 1972.

(44) Glasstone, S.; Laidler, K. J.; Eyring, H. *The Theory of RateProcesses*; McGraw-Hill: New York, 1941.

(45) Stein, S. E.; Rabinovitch, B. S. *J. Phys. Chem.* **1973**, *58*, 2438.

(46) Beyer, T.; Swinehart, D. F. *Commun. ACM* **1973**, *16*, 379.

(47) Rao, V. S.; Skinner, G. B. *J. Phys. Chem.* **1984**, *88*, 5990.

(48) Nicovich, J. M.; Ravishankara, A. R. *J. Phys. Chem.* **1984**, *88*, 2534.

(49) Kiefer, J. H.; Mizerka, L. J.; Patel, M. R.; Wei, H. C. *J. Phys. Chem*. **1985**, *89*, 2013.

(50) Tully, F. P.; Ravishankara, A. R.; Thompson, R. L.; Nicovich, J. M.; Shah, R. C.; Kreutter, N. M.; Wine, P. H. *J. Phys. Chem*. **1981**, *85*, 2262.

(51) (a) Madronich, S.; Felder, W. *J. Phys. Chem.* **1985**, *89*, 3556. (b) Felder, W.; Madronich, S. *Combust. Sci. Technol.* **1986**, *50*, 135.

(52) Atkinson, R. *Chem. Rev.* **1986**, *86*, 69.

(53) Baulch, D. L.; Cobos, C. J.; Cox, R. A.; Esser, C.; Frank, P.; Just, T.; Kerr, J. A.; Pilling, M. J.; Troe, J.; Walker, R. W.; Warnatz, J. *J. Phys. Chem. Ref. Data* **1992**, *21*, 411.

(54) Lorenz, K.; Zellner, R. *Ber. Bunsen-Ges. Phys. Chem.* **1983**, *87*, 629.

(55) Wallington, T. J.; Neuman, D. M.; Kurylo, M. J. *Int. J. Chem. Kinet.* **1987**, *19*, 725.

(56) Krech, M.; Price, J. W. *Can. J. Chem.* **1967**, *45*, 157.

(57) Zhang, H.-X.; Ahonkhai, S. I.; Back. M. H. *Can. J. Chem.* **1989**, *67*, 1541.

(58) Bittner, J. D.; Palmer, H. B.; Howard, J. B. In *Soot Formation in Combustion Systems and Its Toxic Properties*; Lahaye, J., Prado, G., Eds.; Plenum: New York, 1983; p 95.

(59) Hsu, D. S. Y.; Lin, C. Y.; Lin, M. C. *Proc. Int. Symp. Combust.* **1984**, *20*, 623.

(60) (a) Richter, H.; Grieco, W. J.; Howard, J. B. *Combust. Flame* **1999**, *119*, 1. (b) Wang, H.; Frenklach, M. *Combust. Flame* **1997**, *110*, 173.

(61) Violi, A.; Truong, T. N.; Sarofim, A. F. *J. Phys. Chem. A* **2004**, *108*, 4846.

(62) Yu, T.; Lin, M. C.; Melius, C. F. *Int. J. Chem. Kinet.* **1994**, *26*, 1095.

(63) Fahr, A.; Mallard, W. G.; Stein, S. E. *Proc. Int. Symp. Combust.* **1986**, *21*, 825. (b) Fahr, A.; Stein, S. E. *Proc. Int. Symp. Combust.* **1988**, *22*, 1023.

(64) Heckmann, E.; Hippler, H.; Troe, J. *Proc. Int. Symp. Combust.* **1996**, *26*, 543.

(65) Smith, D. M.; Nicolaides, A.; Golding, B. T.; Radom, L. *J. Am. Chem. Soc.* **1998**, *120*, 10223.

(66) Speybroeck, V.; Reyniers, M.-F.; Marin, G. B.; Waroquier, M. *Chem. Phys. Chem.* **2002**, *3*, 863.

(67) Speybroeck, V.; Hemelsoet, K.; Waroquier, M.; Marin, G. B. *Int. J. Quantum Chem.* **2004**, *96*, 568.

(68) Speybroeck, V.; Borremans, Y.; Neck, D.; Waroquier, M.; Wauters, S.; Saeys, M.; Marin, G. B. *J. Phys. Chem. A* **2001**, *105*, 7713.

(69) Deyerl, H.-J.; Fischer, I.; Chen, P. *J. Chem. Phys.* **1999**, *110*, 1450.

(70) Mebel, A. M.; Lin, M. C.; Chakraborty, D.; Park, J.; Lin, S. H.; Lee, Y. T. *J. Chem. Phys.* **2001**, *114*, 8421.

(71) Froese, R. D. J.; Humbel, S.; Svensson, M.; Morokuma, K. *J. Phys. Chem. A* **1997**, *101*, 227.

(72) Froese, R. D. J.; Coxon, J. M.; West, S. C.; Morokuma, K. *J. Org. Chem.* **1997**, *62*, 6991.

CT0500491